Strong Transport of Anthropogenic Carbon from the Antarctic Shelf to Deep Southern Ocean

Shuang Zhang
Jimei University
Yingxu Wu
Jimei University https://orcid.org/0000-0002-7847-6215
Wei-Jun Cai
University of Delaware https://orcid.org/0000-0003-3606-8325
Zhaomin Wang
Hohai University https://orcid.org/0000-0001-7103-6025
Richard Feely
NOAA/PMEL https://orcid.org/0000-0003-3245-3568
Wenju Cai
CSIRO Oceans and Atmosphere https://orcid.org/0000-0001-6520-0829
Yanmin Wang
The Third Institute of Oceanography (TIO)
Chengyan Liu
Southern Marine Science and Engineering Guangdong Laboratory (Zhuhai)
Xichen Li
Institute of Atmospheric Physics, Chinese Academy of Sciences https://orcid.org/0000-0001-6325-6626
Qinghua Yang
Southern Marine Science and Engineering Guangdong Laboratory (Zhuhai)
Minghu Ding
Chinese Academy of Meteorological Sciences
Zhongsheng Xu
Second Institute of Oceanography, Ministry of Natural Resources (MNR)
Kerr Rodrigo
Laboratório de Estudos dos Oceanos e Clima, Instituto de Oceanografia, Universidade Federal do Rio Grande (FURG)
Yiming Luo
Sun Yat-sen University
Xiao Cheng
School of Geospatial Engineering and Science, Sun Yet-Sen University
Liqi Chen

The Third Institute of Oceanography (TIO)
Di Qi (qidi60@qq.com)
Jimei University https://orcid.org/0000-0003-4762-266X

Article

Keywords:

Posted Date: April 5th, 2022

DOI: https://doi.org/10.21203/rs.3.rs-1518438/v1

Strong Transport of Anthropogenic Carbon from the Antarctic Shelf to Deep Southern Ocean

Shuang Zhang[1, 2, 3], Yingxu Wu[1, 2], Wei-Jun Cai[4], Zhaomin Wang[5], Richard A. Feely[6], Wenju Cai[7], Yanmin Wang[2,3], Chengyan Liu[5], Xichen Li[8], QinghuaYang[5], Minghu Ding[9], Zhongsheng Xu[10], Rodrigo Kerr[11], Yiming Luo[5], Xiao Cheng[5], Liqi Chen[1, 2]*, Di Qi[1, 2, 12]*

[1]Polar and Marine Research Institute, Jimei University, Xiamen, Fujian, China

[2]Key Laboratory of Global Change and Marine-Atmospheric Chemistry (GCMAC) of Ministry of Natural Resources (MNR), The Third Institute of Oceanography (TIO), MNR, Xiamen 361005, China

[3]State Key Lab of Marine Environmental Science, Xiamen University, Xiamen, Fujian, China

[4]School of Marine Science and Policy, University of Delaware, Newark, Delaware 19716, USA

[5]Southern Marine Science and Engineering Guangdong Laboratory (Zhuhai), China

[6]Pacific Marine Environmental Laboratory, National Oceanic and Atmospheric Administration, Seattle, WA 98115–6349, USA.

[7]Centre for Southern Hemisphere Oceans Research (CSHOR), CSIRO Oceans and Atmosphere, Hobart, Tasmania, Australia

[8]International Center for Climate and Environment Sciences, Institute of Atmospheric Physics, Chinese Academy of Sciences, Beijing 10029, China

[9]Chinese Academy of Meteorological Sciences, Beijing 100081, China

[10]Key Laboratory of Marine Ecosystem and Biogeochemistry, Second Institute of Oceanography, Ministry of Natural Resources (MNR), Hangzhou, China

[11]Laboratório de Estudos dos Oceanos e Clima, Instituto de Oceanografia, Universidade Federal do Rio Grande (FURG), Av. Itália km 8, Rio Grande, 96203-900, RS, Brazil

[12]Center for Ocean Mega-Science, Chinese Academy of Sciences, Qingdao, 266071, China

*Correspondence to: E-mail: qidi@jmu.edu.cn; chenliqi@tio.org.cn

Flows of dense shelf water are an efficient mechanism for pumping CO_2 to deep ocean along the continental shelf-slope, particularly in the Antarctic Bottom Water (AABW) formation area and its adjacent waters where most of the global bottom water is formed. The global carbon uptake from the atmosphere is estimated to be 200 teragrams carbon per year (Tg C yr^{-1}). However, the contribution from the Antarctic coastal regions to the global carbon budget remains highly uncertain. Here, using an integrated observational dataset, we find that the export of anthropogenic CO_2 from the Pan-Antarctic shelves to deep Southern Ocean is 45~86 Tg C yr^{-1}, equivalent to 22~43% of the global coastal CO_2 uptake, and much higher than previous estimates. The large carbon transport flux causes a decline in deep water pH of 0.0007 ± 0.0002 pH yr^{-1}, far faster than that of any other open ocean deep waters (<0.0002 pH yr^{-1}). Thus, CSP in the AABW formation area is an important pathway for anthropogenic carbon transport into the ocean interior.

Continental shelf regions constitute only 7−10% of the surface area of global open ocean, but have a disproportionately significant role in global carbon budget, accounting for carbon sink of 200 Tg C yr^{-1} (ref. [1]). There are many processes regulating ocean carbon uptake, which are tightly interconnected by processes including air-sea gas exchange, biological activities, physical mixing, and carbon transport[2,3]. The "continental shelf pump (CSP)" (ref. [4]) refers to a combination of processes of uptake of carbon dioxide (CO_2) from the atmosphere and the outflow of CO_2-enriched subsurface waters off the continental shelf towards the deep ocean

beneath the permanent pycnocline by deep convection and isopycnal mixing[2,4,5], isolating the absorbed carbon from the atmosphere for hundreds of years.

Although there is substantial regional variability in the CSP, dependent on geographic characteristics and ocean mixing status, the efficiency of this carbon pump often shows a pattern of increasing uptake in the high-latitude polar oceans[6]. The cold saline waters with high density increase the CSP efficiency and its magnitude[6]. This is particularly true for the Pan-Antarctic shelf-basin areas, where strong convection of surface waters occurs by the formation of Antarctic Bottom Water (AABW) (ref. [7]). The formation of AABW delivers dissolved oxygen (DO) and CO_2 to the deep ocean, and thus contributes to the global carbon cycle, as well as oxygen and nutrient cycles[6,8]. Shelves surrounding the Antarctica contribute substantially to the entire Antarctic carbon sink[9], and it is also characterized by strong biological productivity[10]. However, estimated flux around Antarctic ranges from a source of $+40$ to a sink of -17 Tg C yr^{-1} (refs.[1,11]), and an observation-based flux of CSP in the Antarctic region and its driving mechanisms remain largely unknown[2,12].

The Antarctic shelves are normally categorized into two types: Weddell Sea-like and Amundsen Sea-like, depending on the relative environmental conditions and their efficiency for deep transport[13,14]. The former (also referred to as cold shelf regions) is characterized by cold shelves and thus is conducive to deep-water formation, whereas the latter (referred to as non-cold shelf regions) is flooded by warm Circumpolar Deep Water (CDW) and is unfavorable for bottom formation. The Weddell Sea-like shelves include four main AABW

71 formation sites, Weddell Sea and Ross Sea in the western Antarctica, and Prydz Bay and
72 Adélie Land in the eastern Antarctica.
73
74 In this study, we provide a revised quantification of the air-sea CO_2 fluxes in the
75 Pan-Antarctic coastal regions, which shows a much larger contribution from the Antarctic
76 shelves than previous estimates. We then use the Prydz Bay (PB) to demonstrate the
77 mechanism and magnitude of carbon outflow from shelf to abyssal ocean (i.e., CSP in PB)
78 based on Global Ocean Data Analysis Project database (GLODAPv2.2020) (ref. [15]) database
79 and additional data from the 31st Chinese Antarctic Research Expedition (CHINARE) cruise
80 in 2015. This is followed by an evaluation of the impact by the Pan-Antarctic exported
81 carbon, showing the deep-water acidification that is far faster than in any other open ocean
82 deep waters.
83
84 **Disproportional Pan-Antarctic shelf contribution to global coastal carbon**
85 **uptake**
86 Recent studies have suggested that the high-latitude Southern Ocean (south of 60°S) is a
87 strong sink for atmospheric CO_2 in summer but turns into a neutral status or a weak source on
88 the annual scale[1,11], thus questioning the accuracy of the earlier estimates[1,16] as they were
89 mostly based on open ocean data, which ignored the very limited data in the coastal seas[11,17].
90 Here, we calculate and update the air-sea CO_2 fluxes in the coastal seas of Antarctic
91 (Pan-Antarctic shelf region, >60°S, 3.05×10^6 km^2, Fig. 1) derived from emerging data
92 collected on 27 Antarctic research cruises (Extended Data Table 1 and Methods). We first

93 assume a typical open-water (ice-free) period of four months (~120 days, covering the austral
94 summer from mid-November to mid-March, see Methods)[18]. Then, we divide the shelf into
95 cold shelves regions with four subregions (Fig. 1a, c, e, f) and non-cold shelves regions with
96 another four subregions (Fig. 1b, d, g, h) based on the characteristic of shelves (the outer limit
97 of the shelf was characterized by the shelf break in the south of 60°S), spatial patterns of
98 modified circumpolar deep water (mCDW) intrusion, and the bottom water formation. We
99 then combined the estimates in each subregion to obtain the total flux.
100
101 As a result, the CO_2 flux in the high latitude Pan-Antarctic shelf is -44.0 ± 11.6 Tg C yr^{-1}
102 (negative flux indicates the ocean is a CO_2 sink). This new number greatly alters previous
103 CO_2 sink estimation and re-defines the capacity of Antarctic shelf regions CO_2 adsorption[1,11].
104 Our new estimate accounts for 22% of the global coastal ocean sink (~−200 Tg C yr^{-1}) (ref. [1]).
105 Ice melting alleviates light limitation and thus stimulates intense biological production in
106 these seasonal ice zones during austral summer, resulting in a strong sink of atmospheric CO_2
107 (ref. [19]). The highest CO_2 flux density is found in the main AABW formation areas (cold shelf
108 regions) with -1.45 ± 0.47 mol C m^{-2} yr^{-1} and the total CO_2 flux of cold-shelf regions is −26.8
109 ± 8.6 Tg C yr^{-1} (Extended Data Table 1), accounting for nearly 60% of the Antarctic shelves'
110 capability, indicating that AABW formation areas have major contributions.
111
112 ## CSP delivers anthropogenic carbon into the deep ocean
113 To separate anthropogenic carbon from dissolved inorganic carbon (DIC) in water column,
114 we estimate C_{ant} (from 100 m to the bottom) using two classic tracer approaches, the ΔC*

115 approach and the TrOCA approach[20,21], based on the synthesized data from the Global Ocean
116 Data Analysis Project version 2020 (GLODAPv2.2020) (ref. [15]) and CHINARE 31st cruise.
117 The two approaches show similar results (Fig. 2, Fig. S1), both demonstrating a
118 shelf-to-slope variation of C_{ant}. In addition, we also find that both TrOCA and ΔC*
119 approaches yield comparable C_{ant} estimates of different water masses (Fig. 2) to previously
120 estimated at a few sites in the shelves of the Pan-Antarctic, e.g., DSW in Ross Sea (C_{ant} =
121 20~30 μmol kg^{-1}) (refs. [22,23]) and Adélie Land (C_{ant} = 44 μmol kg^{-1}) (ref. [24]), mCDW and
122 AABW in Weddell Sea (C_{ant} = 10~20 μmol kg^{-1} and 15~20 μmol kg^{-1}, respectively) (ref. [25]).
123 Given that an accurate ΔC* estimation largely depends on nitrate and phosphate
124 concentrations as well as water age determination and that these parameters are usually
125 sparse, we adopt the TrOCA-based results for further discussion in this study.
126
127 Our results show that from the slope to the deep basin, C_{ant} decreases with depth. The overall
128 pattern of C_{ant} distribution in four cold-shelf regions (Fig. 2) appeared to be consistent with
129 the previous estimates based on CFCs in the Southern Ocean[26], suggesting the reliable
130 TrOCA-based results. Maximum C_{ant} concentrations in the shelf waters were in the dense
131 shelf water (DSW), while minimum C_{ant} values were found in the circumpolar deep water
132 (CDW) (Fig. 2), which was characterized by high temperature, salinity, and low DO (ref. [22]).
133 We find that shelf waters have higher C_{ant} concentrations than those in the adjacent basin (Fig.
134 2), but they are still lower than those in other open oceans[25,27]. More importantly, we also find
135 relatively high concentrations of C_{ant} (~15 μmol kg^{-1}) in AABW flowing along the Antarctic
136 slope, below the cores of uncontaminated CDW in the adjacent basin. The concentration of

137 C_{ant} along the AABW generation pathway is higher than those in other marginal seas at
138 low-mid latitudes, e.g. South China Sea (~5 μmol kg^{-1}), East China Sea (~10 μmol kg^{-1}), and
139 western Pacific Ocean (~5 μmol kg^{-1}) (ref. [27]). This is because of the stronger CSP in the
140 Pan-Antarctic, which largely reduces the concentrations of anthropogenic carbon in shelf
141 waters while increasing its inventory in deep waters.
142
143 **Mechanism of CSP in the Prydz Bay**
144 The evolution of CSP originates from the formation of DSW, which is triggered by sea-ice
145 production and brine rejection, and subsequently sinks with absorbed CO_2 from the
146 atmosphere (Fig. 3a). The dense shelf water slips across the shelf break to descend to the
147 deep ocean, where it spreads throughout the global ocean as Antarctic Bottom Water[28]. Prydz
148 Bay is a region of AABW production, and is therefore used as an example to demonstrate the
149 CSP process.
150
151 There are two pathways to transport DSW to the deep ocean in Prydz Bay (Fig. 3a). The
152 primarily DSW flow directly out along the western flank and through Prydz Channel, and
153 then migrate north-westward as a gravity current to ultimately join the very saline DSW from
154 Cape Darnley[29]. The other pathway for DSW is to follow the western flank of the trough/sill,
155 which rises to meet the eastern boundary of the Cape Darnley ice barrier[29]. Both pathways
156 lead to the formation of AABW. As a consequence, the CO_2 absorbed by the upper layer in
157 shelf region is transported to the deep Southern Ocean, with a ventilation rate of 0.26~0.78
158 Sv (1 Sv=10^6 m^3 s^{-1}), accounting for 6~13% of the total AABW formed in the Antarctic[30].

These lines of evidence were further supported by an isotopic perspective revealing the mixing processes between DSW and CDW based on $\delta^{18}O$ and N_2O (Extended Data Fig. 1 and Fig. S2) (refs. [31,32]).

The gross annual flux of anthropogenic CO_2 from the Prydz Bay shelves to AABW can be estimated by the concentration of C_{ant} in DSW and its outflow rate (Eq. 12 in Methods). A total amount of 2.41~7.23 Tg C yr^{-1} (Fig. 3 and Extended Data Table 2) is exported from shelf to deep Southern Ocean by CSP. We also calculate the net C_{ant} export accounting for the source of C_{ant} (although it is almost negligible) from the upwelling of mCDW, i.e., C_{ant} from mCDW contribution subtracted from the gross flux, which is mostly contributed from atmospheric CO_2 absorption. The results in a net C_{ant} flux of 0.40~1.21 Tg C yr^{-1} (Extended Data Table 2), accounting for up to 31% of the air-sea CO_2 uptake (the overall net flux will be discussed later). Such subduction via CSP could also isolate the C_{ant}-rich waters from the atmosphere for centuries[19], and therefore contribute to carbon sequestration.

A greater Pan-Antarctic CSP than previously thought

We subsequently estimated gross fluxes of anthropogenic CO_2 for the other three AABW formation areas, and then integrated them to obtain the total C_{ant} gross fluxes of four cold-shelf regions, which equals 20.6~63.2 Tg C yr^{-1} (Fig. 3b and Extended Data Table 2). Extrapolating this mechanisms of CSP in the four Weddell Sea-like regions to the Pan-Antarctic based on the DSW ventilation rate of Pan-Antarctic (3.70~7.10 Sv) (ref. [33]), all cold-shelf regions in Antarctic would have a C_{ant} gross export flux of 44.7~85.8 Tg C yr^{-1},

which is on the order of 22%~43% of the global coastal sea's net annual uptake of CO_2 (−200 Tg C yr^{-1}, Extended Data Table 2)[1]. Our lower bound is as large as the higher bound of the previous estimates, and our higher bound is almost twice as high. In addition, the four cold-shelf areas account for 46~74% of the C_{ant} gross export fluxes in the Pan-Antarctic, suggesting that there are still some AABW formation regions not included, such as the narrow-continental-shelf coastal polynya regions on the continental margin[34].

We also obtain the net C_{ant} flux for each of Weddell Sea-like regions (Extended Data Table 2). The total net C_{ant} flux of four cold-shelf regions was 9.6~26.2 Tg C yr^{-1}, accounting for 98% of air-sea CO_2 uptake in these regions. The net C_{ant} export flux from the Pan-Antarctic shelves to the deep interior is 18.3~35.2 Tg C yr^{-1}, representing 78% of the Pan-Antarctic air-sea CO_2 uptake. The net C_{ant} export flux and air-sea CO_2 uptake are strongly correlated throughout the Antarctica, implying an influential role of CSP in transferring anthropogenic carbon, which ultimately enhances the uptake capacity of C_{ant} of the shelf waters.

Pan-Antarctic CSP drives strong deep water acidification

The CO_2-rich and low-pH dense water delivered by the continental shelf pump plays a significant role in causing a long-term decline in pH, which is referred to as ocean acidification (OA), as this water mass is transported to the deep basin[2]. We now investigate the long-term trend of pH based on the monthly mean values of each variable.

Notably, from 1974 to 2018, the acidification rate of AABW in four cold-shelf regions

203 averaged about −0.0007 ± 0.0002 yr^{-1} in pH (Fig. 4) (pH in situ was calculated from DIC and
204 TA, though it is lower than that in the surface waters of globally, −0.0017 ± 0.0001 yr^{-1} (ref.
205 [35]), and lower than the rates of pH decline in the surface water of Southern Ocean, −0.0016 ±
206 0.0000 yr^{-1} (ref. [35]). However, this OA rate is faster than those of the deep waters around the
207 world (<−0.0002 yr^{-1}), such as those observed at the Hawaii Ocean Time-series (HOT) and
208 the European Station for Time series in the Ocean at the Canary Island (ESTOC) (refs. [36,37]).
209 We hypothesized that this is because the AABW formation region and the adjacent ocean area
210 have the highest CSP efficiency, which drives a large amount of anthropogenic CO_2 transport
211 into the deep sea.
212
213 To understand the causes behind the observed pH changes presented in Fig. 4, we quantify
214 and decompose the drivers of long-term OA into thermal (driven by temperature change) and
215 non-thermal (driven by salinity, DIC, and TA changes) components (see Methods and Table
216 1). Since temperature barely changed, the pH decrease was mostly caused by non-thermal
217 effect. The main driver of the present-day (1974−2018) pH decrease is the increasing DIC,
218 leading to a decrease in pH of −0.0007 yr^{-1} in AABW, while TA contributes negligibly.
219
220 We further divide ΔDIC into natural effect ($\Delta sDIC\_C_{nat}$) and anthropogenic effect
221 ($\Delta sDIC\_C_{ant} = \Delta sDIC - \Delta sDIC\_C_{nat}$). Our decomposition revealed that the addition of C_{ant}
222 explains around 70% of the observed long-term decrease in pH, whereas the natural carbon is
223 accounting for nearly 30%. The minor impact of natural carbon on acidification suggests a
224 weak sink for natural CO_2 of this area, implying that an important proportion of the

anthropogenic CO_2 flux delivered by CSP, which plays a main part in the anthropogenic CO_2 exchange flux at the air-sea interface. Additionally, the changes of pH driven by anthropogenic CO_2 from 1974 to 2018 (-0.02 ± 0.01, at the rate of -0.0005 ± 0.0001 units yr^{-1}) account for nearly 50% of that from the pre-industrial period to 2018 (-0.04 ± 0.01 see methods), pointing to the rapid the acceleration of acidification rates in the past four decades. Clearly, the absorption and transport of anthropogenic CO_2 are critical in interpreting the acidified AABW which then fuels acidification in the other ocean basins.

Conclusions and implications

The Pan-Antarctic nearshore region has a great capacity and potential for carbon sequestration, especially in the deep-water formation zone. The transport of carbon along shelf and slope to AABW can lead to significant acidification in the deep waters, which threatens the marine ecosystem therein[2]. In the context of global climate change, a reduced outgassing of natural carbon from a weakened overturning of the Southern Ocean[38], a decline of Antarctic sea ice extent and melting of sea ice, as seen after 2015 (ref. [39]), are likely to lead to anomalous advection[40], increased primary productivity[41], and stronger carbon sinks[42], resulting in a potential increase in CSP transport fluxes and exacerbation of deep water acidification in near future. However, an extension of the duration of open water, a weakening of deep convection and formation of AABW due to freshwater input from glacial meltwater[43], a reduction in shelf water export due to warming and freshening[44] will likely represent an opposite effect. Therefore, determining CSP magnitude requires sustained observations. Nevertheless, our study provides a perspective of a greater role by the Antarctic

continental shelf in the global ocean carbon cycle than previously thought, as well as the potential stress on deep-sea ecology in the context of climate change.

References:

1. Roobaert, A. et al. The spatiotemporal dynamics of the sources and sinks of CO_2 in the global coastal ocean. *Global Biogeochemical Cycles* **33**, 1693-1714 (2019).
2. Anderson, L. G. et al. Arctic ocean shelf–basin interaction: An active continental shelf CO_2 pump and its impact on the degree of calcium carbonate solubility. *Deep Sea Research Part I: Oceanographic Research Papers* **57**, 869-879, (2010).
3. Bauer, J. E. et al. The changing carbon cycle of the coastal ocean. *Nature* **504**, 61 (2013).
4. Tsunogai, S., Watanabe, S. & Sato, T. Is there a "continental shelf pump" for the absorption of atmospheric CO_2? *Tellus B: Chemical and Physical Meteorology* **51**, 701-712 (1999).
5. Thomas, H., Bozec, Y., Elkalay, K. & de Baar, H. J. W. Enhanced Open Ocean Storage of CO_2 from Shelf Sea Pumping. *Science* **304**, 1005-1008, (2004).
6. Yool, A. & Fasham, M. J. An examination of the "continental shelf pump" in an open ocean general circulation model. *Global Biogeochemical Cycles* **15**, 831-844 (2001).
7. DeVries, T. The oceanic anthropogenic CO_2 sink: Storage, air-sea fluxes, and transports over the industrial era. *Global Biogeochemical Cycles* **28**, 631-647 (2014).
8. Orsi, A., Johnson, G. & Bullister, J. Circulation, mixing, and production of Antarctic Bottom Water. *Progress in Oceanography* **43**, 55-109 (1999).
9. Arrigo, K. R., van Dijken, G. & Long, M. Coastal Southern Ocean: A strong anthropogenic CO_2 sink. *Geophysical Research Letters* **35**, (2008).
10. Arrigo, K. R., van Dijken, G. L. & Bushinsky, S. Primary production in the Southern Ocean, 1997–2006. *Journal of Geophysical Research: Oceans* **113**, (2008).
11. Lenton, A. et al. Sea-air CO_2 fluxes in the Southern Ocean for the period 1990–2009. *Biogeosciences* **10**, 4037-4054 (2013).
12. Arroyo, M. C., Shadwick, E. H., Tilbrook, B., Rintoul, S. R. & Kusahara, K. A Continental Shelf Pump for CO_2 on the Adélie Land Coast, East Antarctica. *Journal of Geophysical Research: Oceans* **125**, (2020).
13. Petty, A. A., Feltham, D. L. & Holland, P. R. Impact of atmospheric forcing on Antarctic continental shelf water masses. *Journal of Physical Oceanography* **43**, 920-940 (2013).

14. Lee, S. et al. Evidence of minimal carbon sequestration in the productive Amundsen Sea polynya. *Geophysical Research Letters* **44**, 7892-7899 (2017).
15. Olsen, A. et al. GLODAPv2.2020–an update of GLODAPv2. *Earth System Science Data* **11**, 1437-1461 (2020).
16. Friedlingstein, P. et al. Global Carbon Budget 2020. *Earth System Science Data* **12**, 3269-3340, (2020).
17. Bushinsky, S. M. et al. Reassessing Southern Ocean Air-Sea CO_2 Flux Estimates with the Addition of Biogeochemical Float Observations. *Global Biogeochemical Cycles* **33**, 1370-1388 (2019).
18. Roden, N. P., Shadwick, E. H., Tilbrook, B. & Trull, T. W. Annual cycle of carbonate chemistry and decadal change in coastal Prydz Bay, East Antarctica. *Marine Chemistry* **155**, 135-147 (2013).
19. Murakami, K. et al. Strong biological carbon uptake and carbonate chemistry associated with dense shelf water outflows in the Cape Darnley polynya, East Antarctica. *Marine Chemistry* **225**, 103842 (2020).
20. Gruber, N., Sarmiento, J. L. & Stocker, T. F. An improved method for detecting anthropogenic CO_2 in the oceans. *Global Biogeochemical Cycles* **10**, 809-837 (1996).
21. Touratier, F. & Goyet, C. Applying the new TrOCA approach to assess the distribution of anthropogenic CO_2 in the Atlantic Ocean. *Journal of Marine Systems* **46**, 181-197 (2004).
22. Sandrini, S. et al. Anthropogenic carbon distribution in the Ross Sea, Antarctica. *Antarctic Science* **19**, 395-407 (2007).
23. Chen, C. Some indications of excess CO_2 penetration near Cape Adare off the Ross Sea. *Oceanographic Literature Review* **6**, 441 (1994).
24. Shadwick, E. H., Tilbrook, B. & Williams, G. D. Carbonate chemistry in the Mertz Polynya (East Antarctica): Biological and physical modification of dense water outflows and the export of anthropogenic CO_2. *Journal of Geophysical Research: Oceans* **119**, 1-14 (2014).

25. Lo Monaco, C., Goyet, C., Metzl, N., Poisson, A. & Touratier, F. Distribution and inventory of anthropogenic CO_2 in the Southern Ocean: Comparison of three data-based methods. *Journal of Geophysical Research: Oceans* **110**, (2005).
26. Lo Monaco, C., Metzl, N., Poisson, A., Brunet, C. & Schauer, B. Anthropogenic CO_2 in the Southern Ocean: Distribution and inventory at the Indian-Atlantic boundary (World Ocean Circulation Experiment line I6). *Journal of Geophysical Research: Oceans* **110**, (2005).
27. Huang, P. et al. Spatial and temporal trends of anthropogenic carbon storage in typical marginal seas along the Asia continent in the northern hemisphere. *Science of The Total Environment* **823**, 153580, (2022).
28. Gordon, A. L. Bottom water formation. (Associated Press NY, USA, 2009).
29. Williams, G. D. et al. The suppression of Antarctic bottom water formation by melting ice shelves in Prydz Bay. Nature Communications 7, 12577 (2016).
30. Ohshima, K. I. et al. Antarctic Bottom Water production by intense sea-ice formation in the Cape Darnley polynya. *Nature Geoscience* **6**, 235-240 (2013).
31. Fang, Z. et al. Transport of dissolved black carbon from the Prydz Bay Shelf, Antarctica to the deep Southern Ocean. *Limnology and Oceanography* **63**, 2179-2190 (2018).
32. Zhan, L. et al. Austral summer N_2O sink and source characteristics and their impact factors in Prydz Bay, Antarctica. *Journal of Geophysical Research: Oceans* **120**, 5836-5849 (2015).
33. Orsi, A. H., Smethie Jr., W. M. & Bullister, J. L. On the total input of Antarctic waters to the deep ocean: A preliminary estimate from chlorofluorocarbon measurements. *Journal of Geophysical Research: Oceans* **107**, 31-14, (2002).
34. Kitade, Y. et al. Antarctic Bottom Water production from the Vincennes Bay Polynya, East Antarctica. *Geophysical Research Letters* **41**, (2014).
35. Gregor, L. & Gruber, N. Ocean SODA-ETHZ: a global gridded data set of the surface ocean carbonate system for seasonal to decadal studies of ocean acidification. *Earth Syst. Sci. Data* **13**, 777-808 (2021).
36. Chen, C.-T. A. et al. Deep oceans may acidify faster than anticipated due to global warming. *Nature Climate Change* **7**, (2017).

37. Dore, J. E., Lukas, R., Sadler, D. W., Church, M. J. & Karl, D. M. Physical and biogeochemical modulation of ocean acidification in the central North Pacific. *Proceedings of the National Academy of Sciences* **106**, 12235-12240 (2009).
38. DeVries, T., Holzer, M. & Primeau, F. Recent increase in oceanic carbon uptake driven by weaker upper-ocean overturning. *Nature* **542**, 215-218 (2017).
39. Eayrs, C., Li, X., Raphael, M. N. & Holland, D. M. Rapid decline in Antarctic sea ice in recent years hints at future change. *Nature Geoscience* **14**, 460-464 (2021).
40. Landschützer, P. et al. The reinvigoration of the Southern Ocean carbon sink. *Science* **349**, 1221 (2015).
41. Lewis, K. M., van Dijken, G. L. & Arrigo, K. R. Changes in phytoplankton concentration now drive increased Arctic Ocean primary production. Science 369, 198-202 (2020).
42. Brown, M. S. et al. Enhanced oceanic CO_2 uptake along the rapidly changing West Antarctic Peninsula. *Nature Climate Change* **9**, 678-683 (2019).
43. Silvano, A. et al. Freshening by glacial meltwater enhances melting of ice shelves and reduces formation of Antarctic Bottom Water. *Science advances* **4**, eaap9467 (2018).
44. Hellmer, H. H., Kauker, F., Timmermann, R. & Hattermann, T. The Fate of the Southern Weddell Sea Continental Shelf in a Warming Climate. *Journal of Climate* **30**, 4337-4350 (2017).

Figures and figure legends

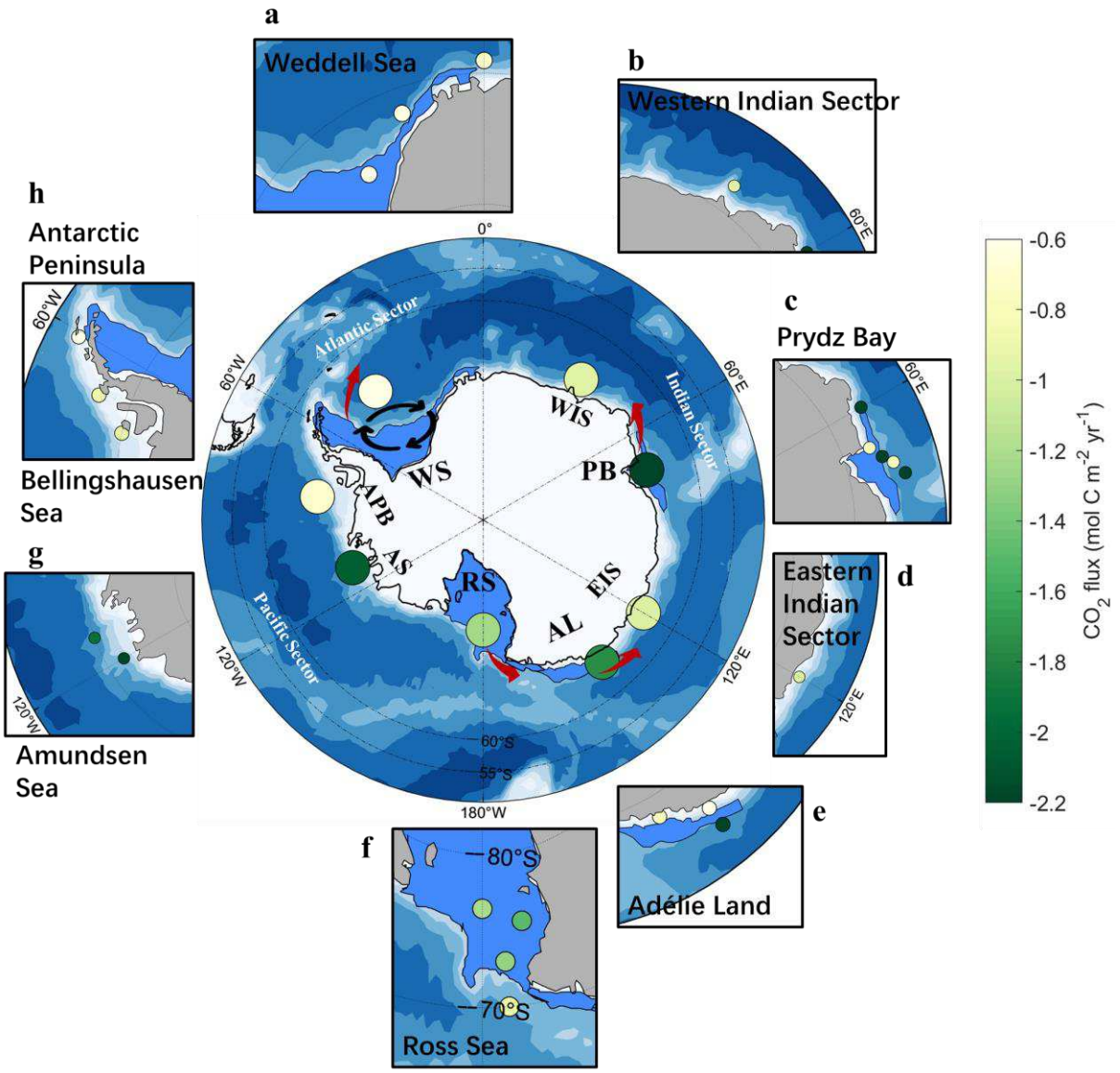

Fig. 1 | The updated annual air-sea CO_2 flux (mol C m^{-2} yr^{-1}) around the Pan-Antarctic. The updated annual air-sea CO_2 flux in the center shows the mean value of CO_2 flux from each sub-region. The separating sub-figures are the CO_2 flux calculated from the daily fluxes that have been reported previously (Extended Data Table 1). The four cold shelves covered by sky-blue patches are **a**, Weddell Sea shelf region (WS), **c**, Prydz Bay shelf region (PB), **e**, Adélie Land shelf region (AL), **f**, Ross Sea shelf region (RS). The non-cold shelf regions are **b**, Western Indian Sector (WIS), **d**, Eastern Indian Sector (EIS), **g**, Amundsen Sea shelf region (AS), **h**, Antarctic Peninsula and Bellingshausen Sea shelf region (APB). The thick red arrows show the direction of AABW formation. Positive values indicate carbon source, negative values indicate carbon sink. Units of flux are in mol C m^{-2} yr^{-1}. Results show a pronounced sink updated in the south of 60°S Pan-Antarctic shelf regions, while the four cold-shelf regions contribute to a strong CO_2 uptake.

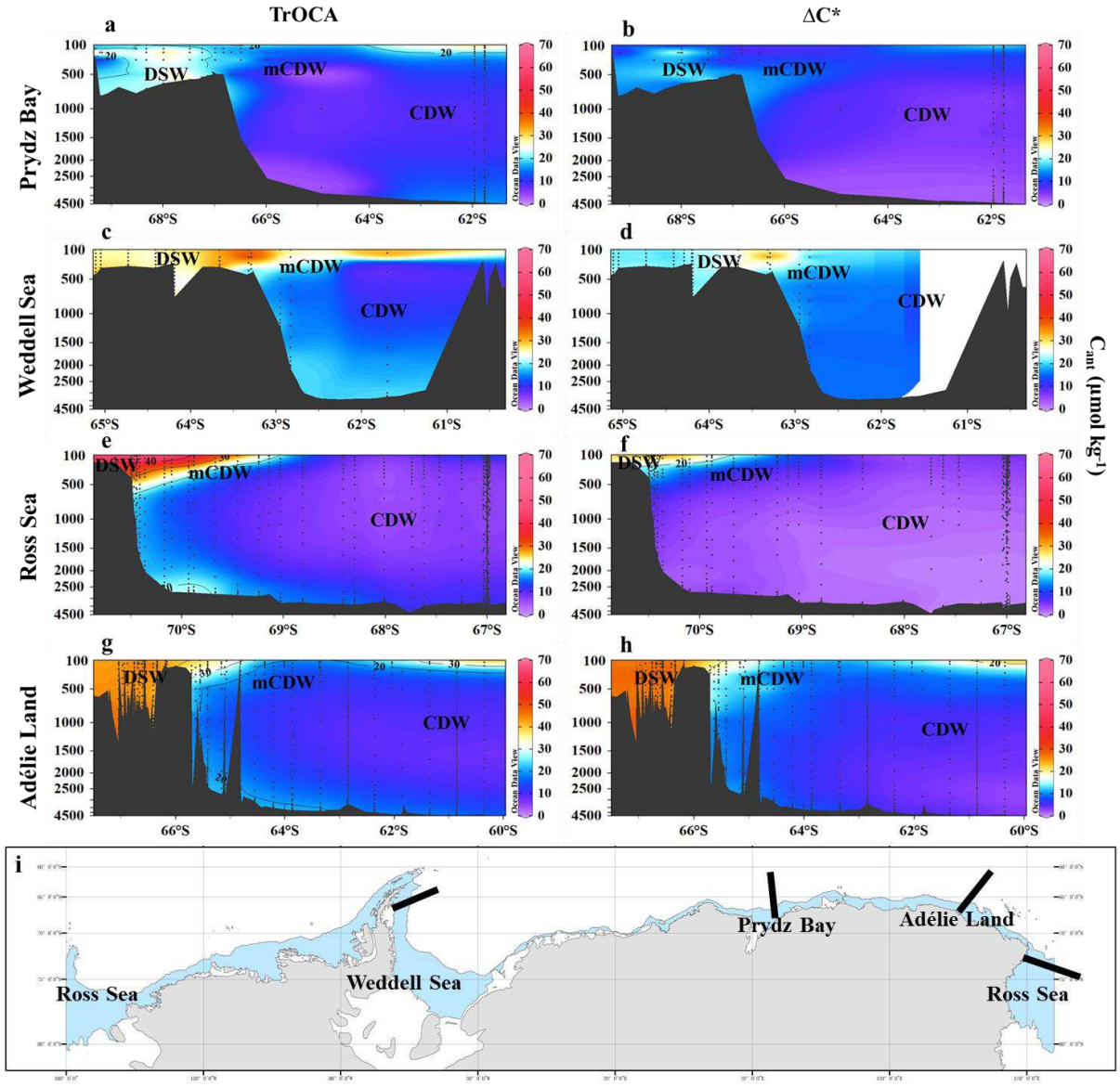

Fig. 2 | The vertical distributions of C_{ant} in the Adélie Land, Weddell Sea, Ross Sea, Prydz Bay using the TrOCA and ΔC* approaches. Four cold shelves are defined as Adélie Land (60°−90°S, 140°−150°E), Weddell Sea (60°−90°S, 0°−60°W), Ross Sea (60°−90°S, 150°−180°E, 160°−180°W) and Prydz Bay (60°−90°S, 60°−80°E). The black bold short solid lines in **i** indicate the sections in figures **a-h**. The Weddell Sea and Ross Sea have the wide continental shelves, the Prydz Bay and Adélie Land have the narrow continental shelves. The different structure of continental shelves means the different residence times for shelf waters and the different shelf-slope systems. Different water masses are defined in Table S1. Results demonstrate higher concentration of C_{ant} along the slope, indicating a high efficient CSP export mechanism.

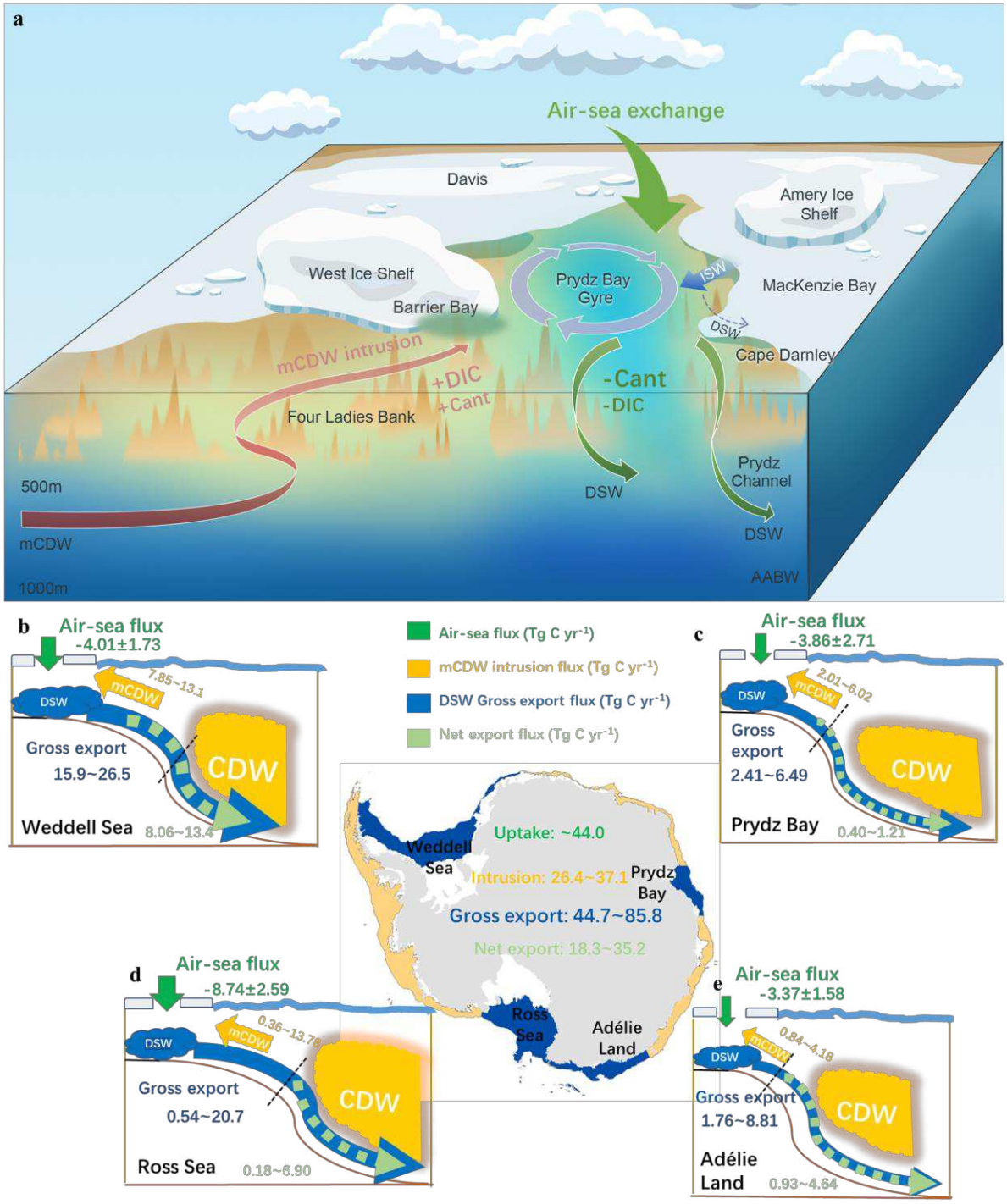

Fig. 3 | An overview of anthropogenic carbon (C_{ant}) exports fluxes in the Pan-Antarctica. **a,** A schematic view of carbon transport in the Prydz Bay. The brine rejection during sea-ice formation in coastal polynyas of Prydz Bay generates DSW, during which process the warmer CDW (also called modified circumpolar deep water, mCDW) intrude onto the shelf. DSW carries C_{ant} downwards along the continental slope, where it entrains CDW continuously and then subducts to form AABW. Thus, strong potential uptake of CO_2 in shelf regions and the AABW formation serve as an efficient vehicle for anthropogenic carbon to the deep Southern Ocean. **b-e,** C_{ant} export fluxes in four cold AABW formation areas, including **b**, Weddell Sea, **c**, Prydz Bay, **d**, Ross Sea, **e**, Adélie Land. Carbon can export both

within DSW (values in blue) and mCDW (values in orange) across the shelf break (black dotted line). The net air-sea CO_2 fluxes are in green (negative values indicate carbon sink) and the net carbon export fluxes are in light green. All C_{ant} fluxes are presented as positive values, arrows indicate direction of flux. The range of numbers in figures is derived from the uncertainty of water mass ventilation rates. By extrapolating the C_{ant} concentrations of the four cold shelves to the entire Pan-Antarctic, we could get the C_{ant} export fluxes of Pan-Antarctic (values in center figure). We show that CSP is an important pathway for the transport of C_{ant} from DSW to AABW in Prydz Bay, which could also be applied to the other cold-shelf systems in the Pan-Antarctic.

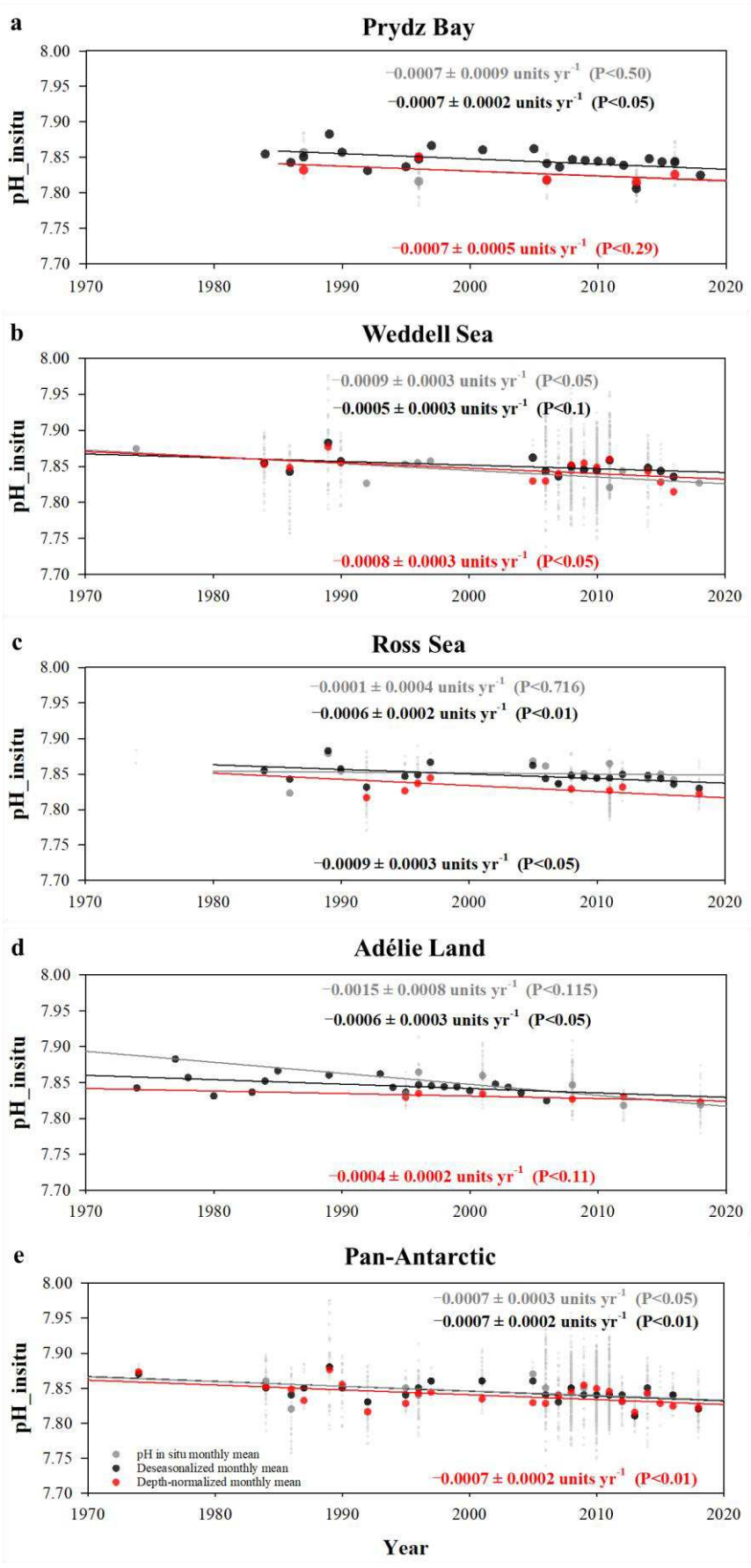
a
Prydz Bay
−0.0007 ± 0.0009 units yr-1 (P<0.50)
−0.0007 ± 0.0002 units yr-1 (P<0.05)
−0.0007 ± 0.0005 units yr-1 (P<0.29)
b
Weddell Sea
−0.0009 ± 0.0003 units yr-1 (P<0.05)
−0.0005 ± 0.0003 units yr-1 (P<0.1)
−0.0008 ± 0.0003 units yr-1 (P<0.05)
c
Ross Sea
−0.0001 ± 0.0004 units yr-1 (P<0.716)
−0.0006 ± 0.0002 units yr-1 (P<0.01)
−0.0009 ± 0.0003 units yr-1 (P<0.05)
d
Adélie Land
−0.0015 ± 0.0008 units yr-1 (P<0.115)
−0.0006 ± 0.0003 units yr-1 (P<0.05)
−0.0004 ± 0.0002 units yr-1 (P<0.11)
e
Pan-Antarctic
−0.0007 ± 0.0003 units yr-1 (P<0.05)
−0.0007 ± 0.0002 units yr-1 (P<0.01)
−0.0007 ± 0.0002 units yr-1 (P<0.01)
pH in situ monthly mean
Deseasonalized monthly mean
Depth-normalized monthly mean
pH_insitu
Year
8.00
7.95
7.90
7.85
7.80
7.75
7.70
1970
1980
1990
2000
2010
2020

407

Fig. 4 | The long-term trends of pH in the deep Southern Ocean (AABW). The dark grey and grey dots indicate the monthly mean of observed pH and the raw observations of pH in **a,** Adélie Land, **b,** Prydz Bay, **c,** Weddell Sea, **d,** Ross Sea, **e,** Pan-Antarctic. The black and red dots indicate the deseasonalized monthly mean pH and the depth-normalized monthly mean pH after deseasonalization, respectively. The dark grey, black, and red solid lines show linear regressions and the rates of change with standard errors are shown in each panel, corresponding to the observed monthly mean, the deseasonalized monthly mean and the depth-normalized monthly mean, respectively. The pH data in **a-e** were obtained from the Global Data Analysis Project version 2020 database. Results show the acidification in AABW in cold-shelf regions due to strong carbon transport by CSP.

Table 1 | Estimated contributions to the long-term pH trends in deep waters of Pan-Antarctic from 1974-2018 and from pre-industrial to 2018.

	Driver	Driver rate of change (yr^{-1})	Changes in drivers (1974~2018)	Contribution to the long-term trends pH (units yr^{-1})
Thermal component	ΔT	−0.00 ± 0.00 ℃	0.05 ± 0.11 ℃	−0.0000 ± 0.0000
Non-thermal Component	ΔsDIC	0.22 ± 0.05 μmol kg^{-1}***	9.73 ± 2.32 μmol kg^{-1}	−0.0007 ± 0.0001
	ΔsDIC_C_{ant}♯	0.16 ± 0.06 μmol kg^{-1}*	6.96 ± 2.68 μmol kg^{-1}	−0.0005 ± 0.0001
	ΔsDIC_C_{nat}♯	0.06 ± 0.07 μmol kg^{-1}	2.77 ± 3.20 μmol kg^{-1}	−0.0001 ± 0.0002
	ΔS	0.00 ± 0.00 ppt	−0.01 ± 0.01 ppt†	0.0000 ± 0.0000
Sum				−0.0007 ± 0.0002

The thermal component and non-thermal component were separated by normalizing the pH to S=34.66 (the mean salinity value of AABW in four regions). The rates (± standard error of slope) were estimated by linear regression using the yearly means. The asterisks indicate the levels of significance of the trends (***$P < 0.001$, **$P < 0.01$, *$P < 0.05$). †Parts per thousand (ppt) measures the salt content in seawater.
♯The ΔDIC_C_{ant} and ΔDIC_C_{nat} means the changes in DIC due to anthropogenic CO_2 and natural CO_2, respectively.

Methods

Discrete DIC and TA data. Water samples throughout the water column were collected using Niskin bottles along six transects from Prydz Bay aboard the R/V XueLong during the 31st Antarctic cruises Chinese National Antarctica Research Expedition (CHINARE 31) from 05 February to 02 March 2015. Potential temperature and salinity data were derived from Seabird-CTD (911 plus). Measurement of carbonate chemistry parameters related to marine carbonate systems followed the "Guide to Best Practices for Ocean CO_2 Measurements"[45]. DIC was measured by AS-C3 Dissolved Inorganic Carbon Analyzer Instruction (Apollo SciTech) and TA was measured by Grand titration. Both DIC and TA were measured with a precision better than 2 μmol kg^{-1}. Accuracy of the measurements was monitored by routine analysis of Certified Reference Materials (CRMs, batch 180, provided by A.G. Dickson, Scripps Institution of Oceanography).

Other DIC and TA data in Prydz Bay, Weddell Sea, Adélie Land, Ross Sea were downloaded from the GLODAPv2.2020 dataset (https://www.glodap.info/index.php/merged-and-adjusted-data-product/).

pH in situ and other related parameters were computed from DIC, TA, temperature, and salinity using the Matlab version of CO2SYS v1.1[46]. Carbonate dissolution constants were taken from Roy et al.[47], K_{sp} from Mucci[48], Kso_4 from Dickson and Millero[49].

Air-sea flux calculation. In Pan-Antarctic (>60°S) shelf regions, early spring and winter often act as weak sources of atmospheric CO_2, because CO_2 outgassing is mostly suppressed by ice cover[50-52]. After accounting for the open water areas and the production, the outgassing flux in early spring and winter is assumed to be offset by compensation in autumn and mid spring[50,51,53], i.e., annual net gas exchange flux at the air-sea interface can approximately equals a four-month CO_2 uptake (~120 days, covering the austral summer from mid-November to mid-March)[18,54,55]. A surface area of each sub-region is calculated using a geographical information system. The off-shore limit of the continental shelf is characterized by the shelf break, whose depth is calculated using a high-resolution global bathymetric database[56,57]. Mean annual air-sea fluxes that from each daily air-sea CO_2 flux and a four-month open water duration, are used to estimate sub-region air-sea CO_2 flux. Average annual flux density (mol C m^{-2} yr^{-1}) is calculated for each sub-region and then is extrapolated to the cold shelf regions and total Pan-Antarctic (>60°S) shelf regions based on the surface areas (see Extended Data Table 1).

Anthropogenic CO_2 calculation – TrOCA approach. The TrOCA (Tracer combining O_2, TCO_2, TA) method initially proposed by Touratier[21,58] to calculate the anthropogenic CO_2 concentration. The conservative tracers TrOCA and $TrOCA^0$ were defined as Eqs. 1−2 and the concentration of anthropogenic CO_2 (C_{ant_TrOCA}) was estimated from Eq. 3 with the assumptions of TA = TA^0 and O_2=O_2^0. $TrOCA^0$ was computed as a function of potential temperature (θ) and TA, deduced from $\Delta^{14}C$ and CFC-11 tracers. $TrOCA^0$ was determined and expressed as Eq. 4 based on the GLODAP world ocean database (http://cdiac.ornl.gov/oceans/glodap/Glodap home.htm). The four parameters are determined by minimizing the fit standard errors of Eq. 4. Thus, the concentration of C_{ant_TrOCA} was estimated as Eq. 5. This method was reported to be conservative in intermediate, deep and

bottom water, and suggested to be suitable for reflecting the combined impact of the air-sea exchange of CO_2 and O_2 (refs. [59,60]). It had previously been applied in the Antarctic regions[22,24,61]. It is noteworthy that the TrOCA method, as well as the other back calculation methods, cannot be applied in the upper mixed layer where biological processes and air-sea CO_2 fluxes modify the upper ocean carbon content on a short time scale. Therefore, we estimated the anthropogenic CO_2 for depths greater than 100 m by the following Eq. 5.

$$TrOCA = O_2 + a\left(DIC - \frac{1}{2}TA\right) \quad (1)$$

$$TrOCA^0 = O_2^0 + a\left(DIC^0 - \frac{1}{2}TA^0\right) \quad (2)$$

$$C_{ant\_TrOCA} = \frac{TrOCA - TrOCA^0}{a} \quad (3)$$

$$TrOCA^0 = e^{\left(b + c\theta + \frac{d}{TA^2}\right)} \quad (4)$$

$$C_{ant\_TrOCA} = \frac{O_2 + 1.279\left(DIC - \frac{1}{2}TA\right) - e^{\left(7.511 - \left(1.087\times10^{-2}\right)\theta - \frac{7.81\times10^5}{TA^2}\right)}}{1.279} \quad (5)$$

Where θ is potential temperature, ℃; O_2 is dissolved oxygen, μmol kg^{-1}; DIC is total inorganic carbon, μmol kg^{-1}; TA is total alkalinity, μmol kg^{-1}; C_{ant_TrOCA} is anthropogenic CO_2 concentration estimated by TrOCA, μmol kg^{-1}. O_2^0, DIC^0 and TA^0 are the natural concentrations of O_2, DIC and TA.

Anthropogenic CO_2 calculation – ΔC^* approach. C_{ant} was also estimated using the classic ΔC^* approach. The quasi-conservative tracer, ΔC^*, was defined as the difference between the measured DIC (C_m), corrected for biology and the preindustrial preformed DIC in equilibrium with the atmosphere (C_{280}), as Eq. 6. The biological term (ΔC_{bio}) included the organic remineralization, the calcium carbonate particles dissolution, and denitrification. The organic component could be estimated by the changes in AOU, together with a stoichiometric ratio and the second component could be got from the difference between the measured TA and a preformed TA (TA^0) as Eq. 7. The TA^0 (Eqs. 8−10) were based on a multiple linear regression fit of surface TA values from different cruises in different oceans[62-64]. The air-sea disequilibrium component (ΔC_{diseq}) could be discriminated from the anthropogenic signal using either information about the water age (by CFC-12) or the distribution of ΔC^* in regions not affected by the anthropogenic transient (as Eq. 11). For given isopycnal surfaces, we assumed that the C_{ant} was zero over some portion of an isopycnal surface, the ΔC_{diseq} was set equal to the average of the ΔC^* values for that portion of the surface according to refs. [62-64]. This method had been applied to the Atlantic Ocean[63,65], the Indian Ocean[64] and the Pacific Ocean[62]. Because Southern Ocean includes three sectors, the Atlantic Sector, the Indian Sector, the Pacific Sector, the ΔC^* calculation used for this study was essentially the same as that modified by Sabine et al. (2002)[62] with one small differences: a combination of

TA^0 (as Eqs. 8−10) and different isopycnal surfaces and their corresponding values of ΔC_{diseq} corresponding to 3 sectors[62-64].

$$\Delta C^* = C_m - \Delta C_{bio} - C_{280} \quad (6)$$

$$\Delta C^* = C_m - C_{280} + 117/170(O - O_{sat}) - 1/2(\mathrm{TA} - \mathrm{TA}^0 - 16/170(O - O_{sat})) + 106/104 N^*_{anom} \quad (7)$$

$$TA^0_{Pacific} = 335.7 + 55.80 * S + 0.08924 * NO \quad (8)$$

$$TA^0_{Indian} = 378.1 + 55.22 * S + 0.0716 * PO - 1.236 * \theta \quad (9)$$

$$TA^0_{Atlantic} = 148.7 + 61.36 * S + 0.0941 * PO - 0.582 * \theta \quad (10)$$

$$C_{ant} = C_m - \Delta C_{bio} - C_{280} - \Delta C_{diseq} = \Delta C^* - \Delta C_{diseq} \quad (11)$$

Where C_{ant} refers to anthropogenic carbon concentration, C_m refers to measured DIC concentration in μmol kg^{-1}, ΔC_{bio} refers to DIC (μmol kg^{-1}) changes resulting from the remineralization of organic matter and dissolution of calcium carbonate particles, C_{280} refers to DIC (μmol kg^{-1}) of waters in equilibrium with an atmospheric CO_2 concentration of 280 μatm, ΔC_{diseq}, refers to air-sea CO_2 difference (i.e., ΔpCO_2) expressed in μmol kg^{-1} of DIC, a term that is assumed to be constant for a given isopycnal surface, and has been evaluated on different isopycnal surfaces in refs. [62-64]. PO and NO are a quasi-conservative tracer introduced by Broecker (1974)[66], and θ is the potential temperature. N^*_{anom} is the N* anomaly from the mean as the denitrification corrections. TA^0 is the preformed alkalinity, which is based on a multiple linear regression fit of surface TA values from different cruises in Atlantic Ocean, Indian Ocean, and Pacific Ocean.

Uncertainty estimation of C_{ant}. Though the intense relationship between C_{ant} values from TrOCA and ΔC*, the large difference do exist between these two C_{ant} values (Fig. S1). Touratier and Sabine[59,62] reported that the random sources uncertainty of TrOCA and ΔC* are 6.25 μmol kg^{-1} and 7.50 μmol kg^{-1} respectively. The TrOCA approach is subjected to random errors from measurements and from predictions ($TrOCA^0$). Estimates of the measurement uncertainties of related variables (DO, TA, DIC, θ) are listed in Table S2. The total uncertainty of measurement and estimation of C_{ant} is determined using a Monte Carlo approach, following refs. [67-69]. For calculation of the uncertainty of C_{ant} (see its function in Methods), we first calculated artificial random errors (normally distributed according to the central limit theorem, with a mean of zero and a standard deviation equal to the accuracy/ uncertainty of measurement) using a random number generator. Then, new variable values (the original ones plus the randomly generated errors) were input into the C_{ant} to calculate new C_{ant} values[46]. By doing this 1000 times, we obtained a set of 1000 different values for every single data point in the dataset. We used the standard deviations of these sets to characterize their individual uncertainties. The overall uncertainty of C_{ant} was 17.07 μmol kg^{-1} (Table S2). The same method is used to estimate the uncertainty of ΔC* approach, 17.96 μmol kg^{-1}. The large uncertainties are associated with some key factors during calculation

processes, such as a steady state in long-term variability of ocean processes, a rough empirical formula to estimate the performed $TrOCA^0$, a rough empirical formula for preformed alkalinity (TA^0), the constant values for ΔC_{diseq} along isopycnal surfaces and so on[21,25,59,62,70].

Qualitative tracer data—$H_2\delta^{18}O$ and ΔN_2O. $H_2\delta^{18}O$ has been used by Fang[31] to trace the potential export of dissolved black carbon and dissolved organic carbon from the shelf to the deep Southern Ocean during DSW formation. The signal of $H_2\delta^{18}O$ in DSW (about −0.68‰) is lower than that in CDW (about −0.12‰) due to the formation of sea ice during austral winter. Due to the limited amount of $H_2\delta^{18}O$ data, we also use N_2O to trace the materials exchange between shelf and slope. As Zhan[32] reported, N_2O concentrations are homogeneously distributed in the shelf waters, with the higher value of N_2O (17.9 nmol L^{-1}) in DSW, in contrast, CDW showed the highest N_2O (19.2 nmol L^{-1}), which can bring N_2O-rich water into contact with the atmosphere immediately following the sea ice retreat during the austral summer. This process of AABW formation can bring the N_2O-depleted water to deeper layers and create a N_2O-undersaturated water column (Fig. S2). Therefore, N_2O can be used as a useful tracer of water mixing between DSW and CDW in Prydz Bay (see Fig. S2 and Extended Data Fig. 1). To better describe N_2O changes during water transportation, we used ΔN_2O (ΔN_2O =N_2O−equilibrium N_2O with respect to atmosphere) as a tracer. The latter one on the right-hand side of the equation was calculated based on Weiss and Price[71].

Calculation of carbon export flux. To produce a conservative estimate of C_{ant} export out of shelf regions (e.g. Prydz Bay), we assumed that DSW derived from shelf regions (Prydz Bay and Cape Darnley) contribute to about 6~13% (0.26~0.78 Sv) of the AABW flux according to ref. [30]. C_{ant} is transported into the ocean interior mostly by DSW transport mainly in wintertime, and the T_{min} layer has been regarded as a proxy for chemical characteristics of the surface mixed layer in austral winter (June to August)[19,24]. Thus, we analyzed variations of C_{ant} statistically along the layer with neutral density (γ_n) γ_n> 28.27 kg m^3 and θ<−1.85℃. As Eq. 12 DSW generation and its diapycnal transport suggests a transport pathway for atmospheric CO_2 that was absorbed in summer into the AABW layer from the shelf regions. Shelf waters supplied by mCDW when it intrudes onto the shelf if we take the shelf waters as a box. Then, the net carbon export fluxes were estimated as Eq. 13.

$$\Delta C_{ant}^{gross-export} = C_{DSW\_ant} * V^{DSW} * \Delta T * \rho^{DSW} * m_c \quad (12)$$

$$\Delta C_{ant}^{net-export} = C_{DSW\_ant} * V^{DSW} * \Delta T * \rho^{DSW} * m_c - C_{mCDW\_ant} * V^{mCDW} * \Delta T * \rho^{mCDW} * m_c \quad (13)$$

Where $\Delta C_{ant}^{gross\text{-}export}$ is the annual C_{ant} transport respectively, V^{DSW} is the annual DSW ventilation rate by volume in the study area (Sv; 10^6 m^3 s^{-1}); ΔT is time (a year). ρ^{DSW} is the mean density of DSW and m_c is the molar mass of carbon (g C mol^{-1}), by multiplying these parameters, to yield annual CO_2^{DSW} values from the shelve region. The net C_{ant} export flux is calculated as the concentrations difference values between DSW and mCDW (Eq. 13, positive values indicate export from shelf region to basin). Here, it is assumed that there's no

586 seasonal variability for C_{ant} in DSW and mCDW.
587
588 **Quantification of long-term AABW pH trends.** Before identifying the long-term trends of
589 pH, we examined the temporal distribution of pH in-situ and noticed that the number of pH
590 observations varies greatly among years and seasons depending on the number and timing of
591 cruises (Fig. 4). To avoid the seasonal biases which might be significantly large in the polar
592 ocean, we developed a deseasonalization calculation as described by Takahashi (2009)[72].
593 Following this method, we estimated the mean rate of change for pH of AABW in four
594 cold-shelf regions by linearly regressing deseasonalized mean monthly values. The difference
595 between a monthly mean and the annual average represents the correction to be applied for
596 deseasonalization of the monthly mean. Assuming that the seasonal variability and hence the
597 deseasonalization corrections remain unchanged with time[72], we obtained the deseasonalized
598 pH and its interannual rate of change.
599 Another issue with the pH observations is spatially unevenly distributed sampling,
600 which may induce bias from the over-weighted impact of highly dense data points
601 concentrated within a certain range of pressure layer. We examined the impact of depth on pH
602 by plotting pH on AABW depths for four cold regions (Fig. S3). One way to reduce this bias
603 is to average the pH measurements into specific depth (the annual depth of AABW, 3435.1 m)
604 and then examine the long-term trends with these temporal-averaged values. The difference
605 between the rates derived from the depth-normalized monthly means and the rates from the
606 deseasonalization monthly indicates the impact of depth (pressure) on pH.
607
608 **Driver of the long-term pH trend in AABW.** To distinguish the causes of the temporal
609 changes in pH, we assumed to the variation of a long-term trend in observed pH is linearity
610 composed of temperature (T), salinity (S), DIC, TA, using a first order Taylor-series
611 deconvolution[73]. Therefore, the change in pH, dpH, could be expressed as Eq. 14[74].
612
613 $$dpH = \frac{\partial pH}{\partial T} \times dT + \frac{\partial pH}{\partial DIC} \times dDIC + \frac{\partial pH}{\partial TA} \times dTA + \frac{\partial pH}{\partial S} \times dS \quad (14)$$

614 $$dpH = \frac{\partial pH}{\partial T} \times dT + \frac{\partial pH}{\partial DIC} \times \frac{S}{S_0} \times d\left(sC_{ant} + sC_{nat}\right) + \frac{\partial pH}{\partial TA} \times \frac{S}{S_0} \times dsTA + \left(\frac{sDIC}{S_0}\frac{\partial pH}{\partial DIC} + \frac{sTA}{S_0}\frac{\partial pH}{\partial TA} + \frac{S}{S_0}\frac{\partial pH}{\partial S} \right) \times dS$$

615 (15)

616 $$\frac{d\Delta^{LT} pH}{dt} = \frac{\partial pH}{\partial T} \times \frac{\Delta^{LT} T}{dt} + \frac{\partial pH}{\partial DIC} \times \frac{S}{S_0} \times \frac{\Delta^{LT}\left(sC_{ant} + sC_{nat}\right)}{dt} + \frac{\partial pH}{\partial TA} \times \frac{S}{S_0} \times \frac{\Delta^{LT} TA}{dt} + \left(\frac{sDIC}{S_0}\frac{\partial pH}{\partial DIC} + \frac{sTA}{S_0}\frac{\partial pH}{\partial TA} + \frac{S}{S_0}\frac{\partial pH}{\partial S} \right) \times \frac{\Delta^{LT} S}{dt}$$

617 (16)

618 Where d indicates the change of the property from the respective norm, the sensitivity of
619 pH to each driver ∂pH/∂T, ∂pH/∂S, ∂pH/∂TA, and ∂pH/∂DIC calculated by allowing a small
620 change (1‰) on temperature, salinity, TA and DIC respectively, while keeping all the other
621 parameters constant (Table S3). We separated the freshwater impacts on DIC and TA from the
622 changes related to ocean internal biogeochemical processes and transport mixing[75-78]. We also
623 separated ΔsDIC into ΔsC_{ant} and natural DIC (ΔsC_{nat}), to determine the anthropogenic impact
624 and natural impact on pH, sC_{nat} values were determined as the difference between sDIC and
625 sC_{ant} in Eq. 15. S and S_0 correspond to the observed and reference salinity (the average values

of S in AABW during 1974−2018). Then the long-term changes in pH, $d\Delta^{LT}pH/dt$ in Eq. 16, were attributable to four drivers.

pH decreases due to anthropogenic CO_2 uptake in AABW. To estimate the acidification of AABW caused by anthropogenic CO_2 from pre-industrial to the present, we used CO2SYS to simulate this process. Here we defined that pH_{pre} was the pH in the pre-industrial period and pH was in the observational period from 1974−2018. Because CO_2 invasion does not affect TA, and we found that the negligible changes in TA, temperature, and salinity during the period, therefore, we assumed that TA, temperature, and salinity are constant. Then, we calculated the changes of pH (ΔpH_{ant}) by removing C_{ant} from DIC and then applying the CO2SYS calculation (Eqs. 17−19). Thus, the resulting ΔpH_{ant} means the impact of C_{ant} on pH from pre-industrial to present. We found that pH had reduced −0.04 ± 0.01 due to the additional anthropogenic CO_2 since pre-industrial period.

$$pH = f(TA, DIC, \mathrm{S}, T) \tag{17}$$

$$pH_{pre} = f(TA, DIC - C_{ant}, S, T) \tag{18}$$

$$\Delta pH_{ant} = pH - pH_{pre} \tag{19}$$

Data Availability

Access to datasets analysed in this study are available from the GLODAPv2 website at https://www.glodap.info/index.php/merged-and-adjusted-data-product/.

References:

45. Dickson, A., Chris, S. & Christian, J. R. Guide to Best Practices for Ocean CO_2 Measurements. *Guide to Best Practices for Ocean CO_2 Measurements* **3**, (2007).
46. van Heuven, S., Pierrot, D., Rae, J., Lewis, E. & Wallace, D. W. R. CO2SYS v 1.1, MATLAB program developed for CO_2 system calculations. ORNL/CDIAC-105b. Carbon Dioxide Information Analysis Center, Oak Ridge National Laboratory, U.S. DoE, Oak Ridge, TN. (2011).
47. Roy, R. N. et al. Determination of the ionization constants of carbonic acid in seawater. *Marine Chemistry* **44**, 249-268 (1993).
48. Mucci, A. The solubility of calcite and aragonite in seawater at various salinities, temperatures, and one atmosphere total pressure. *American Journal of Science* **283**, (1983).
49. Dickson, A. G. & Millero, F. J. A comparison of the equilibrium constants for the dissociation of carbonic acid in seawater media. *Deep Sea Research Part A. Oceanographic Research Papers* **34**, 1733-1743 (1987).
50. Shadwick, E. H. et al. Sea Ice Suppression of CO_2 Outgassing in the West Antarctic Peninsula: Implications for The Evolving Southern Ocean Carbon Sink. *Geophysical Research Letters* **48**, (2021).
51. Gibson, J. A. & Trull, T. W. Annual cycle of fCO_2 under sea-ice and in open water in Prydz Bay, East Antarctica. *Marine Chemistry* **66**, 187-200 (1999).
52. Gray, A. R. et al. Autonomous Biogeochemical Floats Detect Significant Carbon Dioxide Outgassing in the High-Latitude Southern Ocean. *Geophysical Research Letters* **45**, 9049-9057 (2018).
53. Arrigo, K. R. & Van Dijken, G. L. Interannual variation in air-sea CO_2 flux in the Ross Sea, Antarctica: A model analysis. *Journal of Geophysical Research: Oceans* **112**, (2007).
54. Constable, A. J. et al. Climate change and Southern Ocean ecosystems I: how changes in physical habitats directly affect marine biota. *Global change biology* **20**, 3004-3025, (2014).

677 55. DeJong, H. B. & Dunbar, R. B. Air-Sea CO_2 Exchange in the Ross Sea, Antarctica.
678 *Journal of Geophysical Research: Oceans* **122**, 8167-8181 (2017).
679 56. Laruelle, G. G., Lauerwald, R., Pfeil, B. & Regnier, P. Regionalized global budget of the
680 CO_2 exchange at the air-water interface in continental shelf seas. *Global Biogeochemical*
681 *Cycles* **28**, 1199-1214, (2014).
682 57. Laruelle, G. G. et al. Global multi-scale segmentation of continental and coastal waters
683 from the watersheds to the continental margins. *Hydrology and Earth System Sciences* **17**,
684 2029-2051 (2013).
685 58. Touratier, F. & Goyet, C. Definition, properties, and Atlantic Ocean distribution of the
686 new tracer TrOCA. *Journal of Marine Systems* **46**, 169-179 (2004).
687 59. Touratier, F., Azouzi, L. & Goyet, C. CFC-11, ^{14}C and ^{3}H tracers as a means to assess
688 anthropogenic CO_2 concentrations in the ocean. *Tellus B* **59**, 318-325 (2007).
689 60. Yool, A., Oschlies, A., Nurser, G. & Gruber, N. A model-based assessment of the
690 TrOCA approach for estimating anthropogenic carbon in the ocean. *Biogeosciences* **7**,
691 (2010).
692 61. van Heuven, S. M. A. C., Hoppema, M., Huhn, O., Slagter, H. A. & de Baar, H. J. W.
693 Direct observation of increasing CO_2 in the Weddell Gyre along the Prime Meridian
694 during 1973–2008. *Deep Sea Research Part II: Topical Studies in Oceanography* **58**,
695 2613-2635 (2011).
696 62. Sabine, C. et al. Distribution of anthropogenic CO_2 in the Pacific Ocean. *Global*
697 *Biogeochemical Cycles* **16**, 30-31-30-17 (2002).
698 63. Lee, K. et al. An updated anthropogenic CO_2 inventory in the Atlantic Ocean. *Global*
699 *Biogeochemical Cycles* **17**, (2003).
700 64. Sabine, C. L. et al. Anthropogenic CO_2 inventory of the Indian Ocean. *Global*
701 *Biogeochemical Cycles* **13**, 179-198 (1999).
702 65. Gruber, N. Anthropogenic CO_2 in the Atlantic Ocean. *Global Biogeochemical Cycles* **12**,
703 165-191 (1998).
704 66. Broecker, W. S. “NO”, a conservative water-mass tracer. *Earth and Planetary Science*
705 *Letters* **23**, 100-107 (1974).

67. Wu, Y., Hain, M., Humphreys, M., Hartman, S. & Tyrrell, T. What drives the latitudinal gradient in open-ocean surface dissolved inorganic carbon concentration? *Biogeosciences* **16**, 2661-2681 (2019).
68. Jouandet, M. P. et al. A seasonal carbon budget for a naturally iron-fertilized bloom over the Kerguelen Plateau in the Southern Ocean. *Deep Sea Research Part II: Topical Studies in Oceanography* **55**, 856-867 (2008).
69. Ribas-Ribas, M. et al. Intercomparison of carbonate chemistry measurements on a cruise in northwestern European shelf seas. *Biogeosciences* **11**, 4339-4355 (2014).
70. Monaco, C. L., Goyet, C., Metzl, N., Poisson, A. & Touratier, F. Distribution and inventory of anthropogenic CO_2 in the Southern Ocean: Comparison of three data-based methods. *Journal of Geophysical Research* **110**, (2005).
71. Weiss, R. F. & Price, B. A. Nitrous oxide solubility in water and seawater. *Marine Chemistry* **8**, 347-359 (1980).
72. Takahashi, T. et al. Climatological mean and decadal change in surface ocean pCO_2, and net sea–air CO_2 flux over the global oceans. *Deep Sea Research Part II: Topical Studies in Oceanography* **56**, 554-577 (2009).
73. Kwiatkowski, L. & Orr, J. C. Diverging seasonal extremes for ocean acidification during the twenty-first century. *Nature Climate Change* **8**, 141-145 (2018).
74. Ouyang, Z. et al. Sea-ice loss amplifies summertime decadal CO_2 increase in the western Arctic Ocean. *Nature Climate Change* (2020).
75. Keeling, C. D., Brix, H. & Gruber, N. Seasonal and long-term dynamics of the upper ocean carbon cycle at Station ALOHA near Hawaii. *Global Biogeochemical Cycles* **18**, (2004).
76. Lovenduski, N. S., Gruber, N., Doney, S. C. & Lima, I. D. Enhanced CO_2 outgassing in the Southern Ocean from a positive phase of the Southern Annular Mode. *Global Biogeochemical Cycles* **21**, (2007).
77. Hauri, C. et al. Spatiotemporal variability and long-term trends of ocean acidification in the California Current System. *Biogeosciences* **10**, 193-216 (2013).

78. García-Ibáñez, M. I., Bates, N. R., Bakker, D. C. E., Fontela, M. & Velo, A. Cold-water corals in the Subpolar North Atlantic Ocean exposed to aragonite undersaturation if the 2°C global warming target is not met. *Global and Planetary Change* **201**, 103480 (2021).
79. Hoppema, M., Fahrbach, E., Stoll, M. H. & de Baar, H. J. Annual uptake of atmospheric CO_2 by the Weddell Sea derived from a surface layer balance, including estimations of entrainment and new production. *Journal of Marine Systems* **19**, 219-233 (1999).
80. Hoppema, M., Stoll, M. H. C. & de Baar, H. J. W. CO_2 in the Weddell Gyre and Antarctic Circumpolar Current: austral autumn and early winter. *Marine Chemistry* **72**, 203-220 (2000).
81. Brown, P. J. et al. Carbon dynamics of the Weddell Gyre, Southern Ocean. *Global Biogeochemical Cycles* **29**, 288-306 (2015).
82. Bates, N. R., Hansell, D. A., Carlson, C. A. & Gordon, L. I. Distribution of CO_2 species, estimates of net community production, and air-sea CO_2 exchange in the Ross Sea polynya. *Journal of Geophysical Research: Oceans* **103**, 2883-2896 (1998).
83. Sweeney, C. in Biogeochemistry of the Ross Sea, 295-312 (2003).
84. Ishii, M., Inoue, H. Y. & Matsueda, H. Net community production in the marginal ice zone and its importance for the variability of the oceanic pCO_2 in the Southern Ocean south of Australia. *Deep Sea Research Part II Topical Studies in Oceanography* **49**, 1691-1706 (2002).
85. Shadwick, E. et al. Glacier tongue calving reduced dense water formation and enhanced carbon uptake. *Geophysical Research Letters* **40**, 904-909 (2013).
86. Shetye, S., Jena, B. & Mohan, R. Dynamics of sea-ice biogeochemistry in the coastal Antarctica during transition from summer to winter. *Geoscience Frontiers* **8**, 507-516 (2017).
87. Wang, Y. et al. Biological and physical controls of pCO_2 and air-sea CO_2 fluxes in the austral summer of 2015 in Prydz Bay, East Antarctica. *Marine Chemistry*, 103897 (2020).
88. Tortell, P. D. et al. Spatial distribution of pCO_2, ΔO_2/Ar and dimethylsulfide (DMS) in polynya waters and the sea ice zone of the Amundsen Sea, Antarctica. *Deep Sea Research Part II: Topical Studies in Oceanography* **71**, 77-93 (2012).

764 89. Mu, L., Stammerjohn, S. E., Lowry, K. E. & Yager, P. L. Spatial variability of surface
765 pCO_2 and air-sea CO_2 flux in the Amundsen Sea Polynya, Antarctica. *Elementa: Science*
766 *of the Anthropocene* **3**, (2014).
767 90. Álvarez, M., Ríos, A. F. & Rosón, G. Spatio-temporal variability of air–sea fluxes of
768 carbon dioxide and oxygen in the Bransfield and Gerlache Straits during Austral summer
769 1995–96. *Deep Sea Research Part II: Topical Studies in Oceanography* **49**, 643-662
770 (2002).
771 91. Legge, O. J. et al. The seasonal cycle of ocean-atmosphere CO_2 flux in Ryder Bay, west
772 Antarctic Peninsula. *Geophysical Research Letters* **42**, 2934-2942 (2015).
773 92. Ito, R. G., Tavano, V. M., Mendes, C. R. B. & Garcia, C. A. E. Sea-air CO_2 fluxes and
774 pCO_2 variability in the Northern Antarctic Peninsula during three summer periods
775 (2008–2010). *Deep Sea Research Part II: Topical Studies in Oceanography* **149**, 84-98
776 (2018).
777 93. Roden, N. P., Tilbrook, B., Trull, T. W., Virtue, P. & Williams, G. D. Carbon cycling
778 dynamics in the seasonal sea-ice zone of East Antarctica. *Journal of Geophysical*
779 *Research: Oceans* **121**, 8749-8769 (2016).
780 94. Nelson, D. M., DeMaster, D. J., Dunbar, R. B. & Smith Jr., W. O. Cycling of organic
781 carbon and biogenic silica in the Southern Ocean: Estimates of water-column and
782 sedimentary fluxes on the Ross Sea continental shelf. *Journal of Geophysical Research:*
783 *Oceans* **101**, 18519-18532 (1996).
784 95. Tozawa, M. et al. Seasonal variations and drivers of surface ocean pCO_2 in the Seasonal
785 Ice Zone of the Eastern Indian Sector, Southern Ocean. *Journal of Geophysical Research:*
786 *Oceans* (2021).
787 96. Foldvik, A. et al. Ice shelf water overflow and bottom water formation in the southern
788 Weddell Sea. *Journal of Geophysical Research: Oceans* **109**, (2004).
789 97. Huhn, O. et al. Evidence of deep- and bottom-water formation in the western Weddell
790 Sea. *Deep Sea Research Part II: Topical Studies in Oceanography* **55**, 1098-1116
791 (2008).
792 98. Whitworth III, T. & Orsi, A. H. Antarctic Bottom Water production and export by tides
793 in the Ross Sea. *Geophysical Research Letters* **33**, (2006).

99. Williams, G. D. et al. Antarctic Bottom Water from the Adélie and George V Land coast, East Antarctica (140–149°E). *Journal of Geophysical Research: Oceans* **115**, (2010).

Acknowledgments This work was supported by the National Key Research and Development Program of China (2019YFE0114800), National Natural Science Foundation of China (41630969, 41806222, 41941013, 42106222 and 42076225), Key Deployment Project of Centre for Ocean Mega-Research of Science, CAS (Grant No. COMS2020Q12), and Natural Science Foundation of Fujian Province, China (2020J05075). We are thankful to the crews of the Chinese National Arctic Research Expedition on board R/V *Xuelong*, as well as National Arctic and Antarctic Data Center from China. We thank Zhengbing Han and Jianming Pan, from the Second Institute of Oceanography, Ministry of Natural Resources, China, for offering the data of nutrients and the dissolved oxygen (DO). We also thank N_2O data offered by Dr. Liyang Zhan.

Author Contributions

D. Q. and L. C designed the program, J. L. and W-YM executed the fieldwork. S. Z. and D.Q. did data processing and drafted the manuscript. S. Z, D. Q. and Y.W. revised the paper. All authors contributed to discussion and writing.

Competing financial interests The authors declare no competing financial interests

Additional information

Extended data is available for this paper.

Supplementary information is available in the online version of the paper.

Extended Data for

Strong Transport of Anthropogenic Carbon from the Antarctic Shelf to Deep Southern Ocean

Shuang Zhang[1, 2, 3], Yingxu Wu[1, 2], Weijun Cai[4], Zhaomin Wang[5], Richard A. Feely[6], Wenju Cai[7], Yanmin Wang[2,3], Chengyan Liu[5], Xichen Li[8], QinghuaYang[5], Minghu Ding[9], Zhongsheng Xu[10], Rodrigo Kerr[11], Yiming Luo[5], Xiao Cheng[5], Liqi Chen[1, 2]*, Di Qi[1, 2, 12]*

[1]Polar and Marine Research Institute, Jimei University, Xiamen, Fujian, China
[2]Key Laboratory of Global Change and Marine-Atmospheric Chemistry (GCMAC) of Ministry of Natural Resources (MNR), The Third Institute of Oceanography (TIO), MNR, Xiamen 361005, China
[3]State Key Lab of Marine Environmental Science, Xiamen University, Xiamen, Fujian, China
[4]School of Marine Science and Policy, University of Delaware, Newark, Delaware 19716, USA
[5]Southern Marine Science and Engineering Guangdong Laboratory (Zhuhai), China
[6]Pacific Marine Environmental Laboratory, National Oceanic and Atmospheric Administration, Seattle, WA 98115–6349, USA.
[7]Centre for Southern Hemisphere Oceans Research (CSHOR), CSIRO Oceans and Atmosphere, Hobart, Tasmania, Australia
[8]International Center for Climate and Environment Sciences, Institute of Atmospheric Physics, Chinese Academy of Sciences, Beijing 10029, China
[9]Chinese Academy of Meteorological Sciences, Beijing 100081, China
[10]Key Laboratory of Marine Ecosystem and Biogeochemistry, Second Institute of Oceanography, Ministry of Natural Resources (MNR), Hangzhou, China
[11]Laboratório de Estudos dos Oceanos e Clima, Instituto de Oceanografia, Universidade Federal do Rio Grande (FURG), Av. Itália km 8, Rio Grande, 96203-900, RS, Brazil
[12]Center for Ocean Mega-Science, Chinese Academy of Sciences, Qingdao, 266071, China

*Correspondence to: E-mail: qidi@jmu.edu.cn; chenliqi@tio.org.cn

This PDF file includes:

Extended Data Figure 1
Extended Data Table 2
Extended Data References

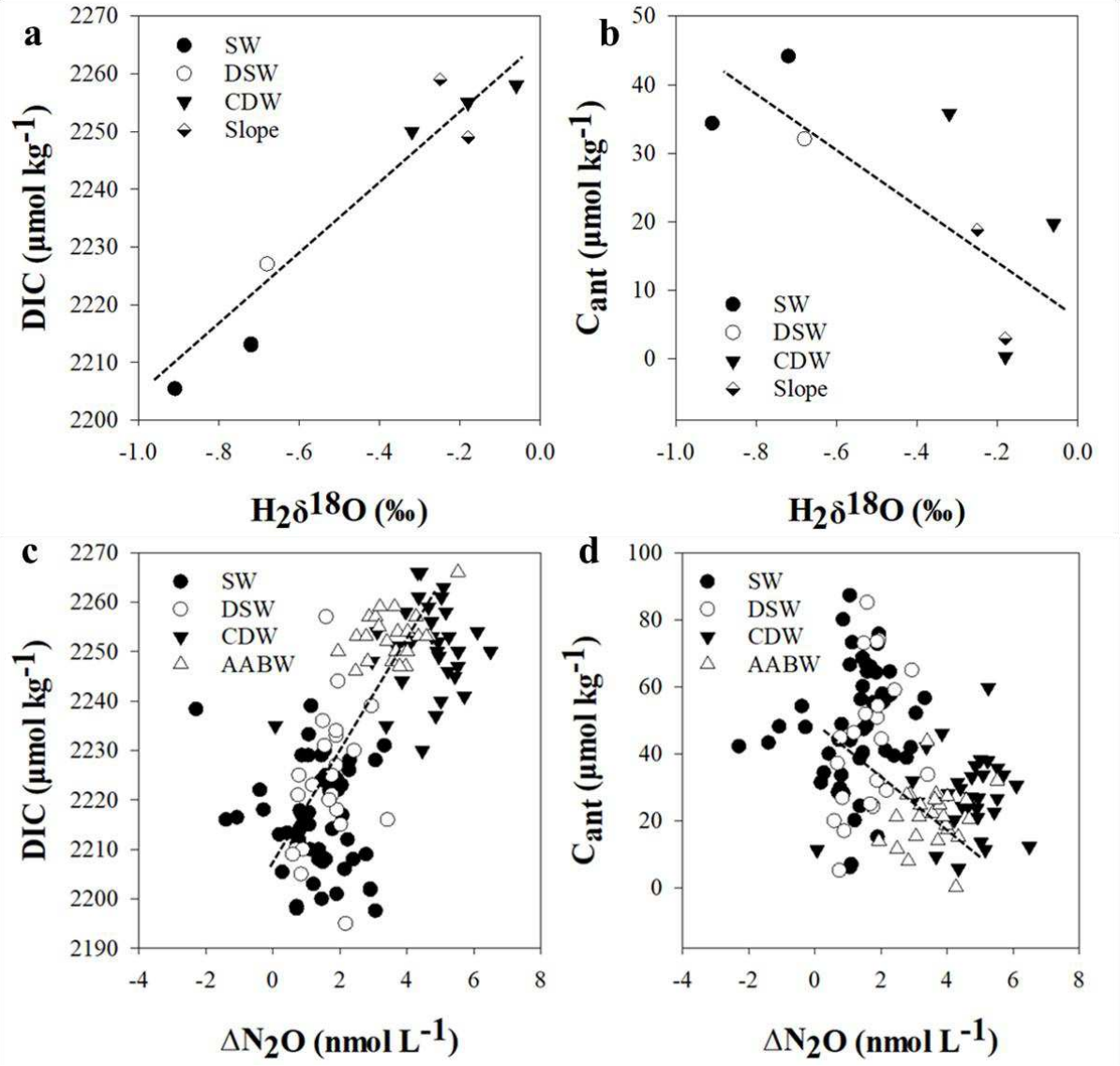

Extended Data Fig. 1 Tracing the mixing process between different water masses by the $H_2\delta^{18}O$ and N_2O in shelf-slope systems. The upper layer is $H_2\delta^{18}O$ vs. **a,** DIC and **c,** C_{ant} and the lower layer is ΔN_2O vs. **b,** DIC and **d,** C_{ant} in Shelf Water (SW), Dense Shelf Water (DSW), Circumpolar Deep Water (CDW), and Antarctic Bottom Water (AABW). The black triangles represent CDW (including mCDW). The mixing line described the downward transport of C_{ant} and the inverse transport of DIC between CDW and DSW, with more negative $\delta^{18}O$ (H_2O) value of DSW (−0.68‰) than CDW (−0.12‰), and lower ΔN_2O (disequilibrium of N_2O with respect to atmosphere value) concentration in DSW (1.7 ± 0.7 nmol L^{-1}) than that in CDW (4.7 ± 0.9 nmol L^{-1}). Therefore, as DSW pass by the shelf break and downward along the slope to form AABW, C_{ant} and DIC were brought to the deep Southern Ocean. Oxygen isotope was collected from Fang[31] and N_2O was provided by Zhan that sampled from the CHINARE 31st (2015).

Extended Data Table 1 Regional estimates of daily and annual air-sea fluxes of CO_2 in the Antarctic coastal seas. Based on the previous syntheses, we further assessed such fluxes by including the most up-to-date flux measurements.

References	Longitude	Latitude	Year	Subregions	Area ($\times10^6$ km^2)	CO_2 flux (mmol m^{-2} d^{-1})	CO_2 flux (g C m^{-2} yr^{-1})	CO_2 flux (mol C m^{-2} yr^{-1})	Total CO_2 flux (Tg C yr^{-1})
		60°-80°			***Cold Shelf Regions (CSR)***				
[79]	60°W–15°E	60°–75°S	1996;1993	Weddell Sea	1.70	−3.27 ± 2.86	−4.71 ± 4.12	−0.39 ± 0.34	−8.00 ± 7.00**a**
[80]	10°W–10°E	61.4°–75°S	1992;1996	Southern Weddell Gyre	–	−5.89**a**	−8.48	−0.71	–
[81]	60°W–30°E	55°–75°S	2008–2010	Weddell Sea	6.20	−3.70 ± 2.35	−5.32 ± 3.39	−0.44 ± 0.28	−33.00 ± 21.00**b**
				Average	**0.65**	**−4.29 ± 3.70**	**−6.17 ± 0.11**	**−0.51 ± 0.22**	**−4.01 ± 1.73**
[82]	171°W–168°E	76.5°S	1994–1996	Ross Sea	0.33	−10.20**c**	−14.69	−1.22	−4.85
[83]	165°–180°E	73°–78°S	1997–2003	Ross Sea	0.44	−12.5 ± 8.33	−18.0 ± 12.0	−1.50 ± 1.00**d**	−7.92 ± 5.28
[55]	160°E–155°W	71°–79°S	2003–2013	Ross Sea	0.47	−10.8 ± 0.83	−15.6 ± 1.2	−1.30 ± 0.10**e**	−7.33± 0.56
[55,56]	160°E–155°W	65°–80°S	1990–2011	Ross Sea	0.47	−7.67 ± 3.67	−11.0 ± 5.28	−0.92 ± 0.44**e**	−5.19± 2.48
				Average	**0.59**	**−10.3 ± 3.05**	**−14.8 ± 0.62**	**−1.24 ± 0.37**	**−8.74 ± 2.59**
[84]	140°E	64°–68°S	1994/95	Adélie Land	–	−2.30 ± 2.30**f**	−3.31 ± 3.31	−0.28 ± 0.28	–
[24,85]	132°–150°E	64°–68°S	1999,2001,2008,2011	Adélie Land	–	−35.0 ± 20.0**g**	−50.4 ± 28.8	−4.20 ± 2.40	–
[12]	140°–150°E	65.5°–68.5°S	2015,2017	Adélie Land	–	−6.56 ± 4.33**h**	−9.45 ± 6.24	−0.79 ± 0.52	–
				Average	**0.16**	**−14.6 ± 6.86**	**−21.1 ± 4.04**	**−1.75 ± 0.82**	**−3.37 ± 1.58**
[51]	78.9°E	68.6°S	1993–1995	Prydz Bay	–	−32.8**i**	−47.23	−3.94	–
[18]	78.8°–78°E	68.5°–68.6°S	2010–2011	Prydz Bay	–	−6.56 ± 4.33**j**	−9.54 ± 6.24	−0.79 ± 0.52	–
[86]	20°–70°E	60°–72°S	2009–2012	Basin	–	−28.4 ± 45.6**k**	−40.9 ± 65.7	−3.41 ± 5.47	–
[19]	67°–71°E	66°–68°S	2009	Cape Darnley Polynya	0.01	−6.50 ± 6.90**l**	−9.36 ± 9.94	−0.78 ± 0.83	−0.13 ± 0.14
[87]	68°–78°E	64°–70°S	2014–2015	Prydz Bay	0.08	−21.4 ± 27.3**m**	−30.8 ± 38.3	−2.57 ± 3.28	−2.47 ± 3.14

Extended Data Table 1: (continued)

				Average	**0.14**	**−15.8 ± 13.4**	**−27.6 ± 6.14**	**−2.30 ± 1.61**	**−3.86 ± 2.71**
				Total of CSR	**1.54**	**−12.1 ± 6.8**	**−17.4 ± 1.84**	**−1.45 ± 0.47**	**−26.8 ± 8.6**
		60°-80°				***Non-Cold Shelf Regions (NCSR)***			
88	95°−125°W	68°−75°S	2009.1−2	Amundsen Sea	0.05	−15.9 ± 13.8**n**	−22.9 ± 19.9	−1.91 ± 1.66	−1.14 ± 0.99
89	109°−122°W	71°−73.7°S	2010−2011	Amundsen Sea Polynya	0.03	−18.0 ± 14.0**o**	−25.9 ± 20.2	−2.16 ± 1.68	−0.78 ± 0.60
				Average	**0.25**	**−17.0 ± 9.8**	**−24.4 ± 2.89**	**−2.03 ± 1.18**	**−6.10 ± 3.54**
90	58°−66°W	62°−65.5°S	1995−1996	Bellingshausen Sea	0.07	−7.55 ± 6.62**p**	−10.9 ± 9.53	−0.91 ± 0.79	−0.76 ± 0.67
91	68.4°−68.1°W	67.57°−67.63°S	2011−2013	WAP (Ryder Bay)	1.20×10^{-4}	−7.50 ± 4.58	−10.8 ± 6.60	−0.90 ± 0.55**q**	−
92	45°−65°W	60°−65°S	2008−2010	NAP	0.32	−1.07 ± 1.30**r**	−1.54 ± 1.87	−0.13 ± 0.16	−0.49 ± 0.60
				Average	**0.59**	**−5.92 ± 3.52**	**−8.55 ± 4.77**	**−0.71 ± 0.42**	**−5.04 ± 2.99**
93	30°−80°E	60°−69°S	2009−2012	**Eastern Indian Sector**	**0.16**	**−8.00 ± 21.0s**	**−12.0 ± 1.82**	**−1.00 ± 2.52**	**−1.84 ± 2.93**
86	80°−150°E	60°−70°S	2018−2019	**Western Indian Sector**	**0.30**	**−6.35 ± 0.64k**	**−9.14 ± 0.92**	**−0.76 ± 0.08**	**−2.74 ± 0.28**
				Total of NCSR	**1.31**	**−9.40 ± 7.2**	**−13.5 ± 4.79**	**−1.13 ± 0.49**	**−17.7 ± 7.8**
				Pan-Antarctic	**2.85**			**−1.29 ± 0.34**	**−44.0 ± 11.6**
						Antarctic Shelves & Southern Ocean			
11		58°−75°S	1990−2009	Antarctic shelf region	23.60		−1.69	−0.14	40.00
6		65°−80°S	−	Antarctic Shelves	2.95	−	−	−	−5.38
3		>45°S	1998−2015	Coastal seas in SO	−	−	−	−	−17.00
17	Southern Ocean	>35°S	1982−2017	SO	−	−	−	−	−750~−1100
						Global Coastal Seas & Global Ocean			
1			1998−2015	Global Coastal Seas	24.73*	−	−8.09	−0.67	−200
1			1998−2015	Global Ocean	335*	−	−5.07	−0.42	−1700

Note: North Antarctic Peninsula (NAP); West Antarctic Peninsula (WAP); Western Antarctic Shelves (WAS); Eastern Antarctic Shelves (EAS); Southern Ocean (SO).

a.*Hoppema et al.* (1999)[79] report the net CO_2 uptake is −8.00 ± 7.00 Tg C yr^{-1}, determined by the difference between entrainment and biological activity based on the balance of surface layer (100 m) of the offshore Weddell Sea. Data from two cruises on the transect between Kapp

Norvegia and Joinville Island at the tip of the Antarctic Peninsula in April/May 1996 and December/January 1993. The surface area of the southwestern sector of the Weddell Sea region is 1.70×10^6 km^2, excluding the shelf areas. The resulting net CO_2 uptake flux is -0.39 ± 0.34 mol C m^{-2} yr^{-1}. Hoppema et al., (2000)[80] report the net CO_2 uptake is -5.89 mmol CO_2 m^{-2} d^{-1} of southern Weddell Sea.

b.*Brown et al.* (2015)[81] report a net annual mean air-sea CO_2 flux -33 ± 21 Tg C yr^{-1} from the surface layer carbon balance method, which is calculated from both the full (1998-2011) and truncated (2008−2010) data sets, the entire Weddell region surface area is 6.20×10^6 km^2, which is extend from the Antarctic Peninsula eastward to 30°E.

c.*Bates et al.* (1998)[82] report a value of -10.20 mmol CO_2 m^{-2} d^{-1} for the ice-free period (from mid-December to mid-February each year) based on two cruises to Ross Sea polynya during November-December 1994 and December 1995 to January 1996. the open water period is nearly 4 months, a ~0.33×10^6 km^2 area that covers 75~80% of the Ross Sea shelf[94].

d.*Sweeney* (2003)[83] calculate the annual air-sea flux of CO_2, -1.5 ± 1.0 mol C m^{-2} from the surface data and sea ice concentrations along the 76.5°S in the Southwestern Ross Sea, which is the sum of bloom period flux (Mid Oct. − Mar.) and winter gas flux (Mar. − Mid Oct.).

e.*DeJong and Dunbar* (2017)[55] calculate CO_2 flux rates with in situ and wind speed data from 20 cruises in the Ross Sea region (160°E–155°W, 71°S–79°S) and find that the Ross Sea is an atmospheric CO_2 sink with -1.30 ± 0.1 mol C m^{-2} yr^{-1}. They also report a more moderate atmospheric CO_2 sink (-0.92 ± 0.44 mol C m^{-2} yr^{-1}), based on Laruelle et al. (2014)[56] during 1990−2011.

f.*Ishii et al.* (2002)[84] calculate the air-sea CO_2 flux of seasonal ice zone (SIZ, the south of 64°S around 140°E) during cruise in the austral summer of 1994/95, from -3.50 ± 2.80 mmol C m^{-2} d^{-1} in December to -1.10 ± 1.70 mmol C m^{-2} d^{-1} in January.

g.*Shadwick et al.* (2013, 2014)[24,85] report a CO_2 flux of -15.00 mmol C m^{-2} d^{-1} in summer 2007/2008 and -30.00~-80.00 mmol C m^{-2} d^{-1} in 2011. Here we take the average flux, -35.0 ± 20.0 mmol C m^{-2} d^{-1}. The surface area of ice-free region is 0.08×10^6 km^2.

h.*Arroyo et al.* (2020)[12] report an average flux of approximately -6.56 ± 4.33 mmol C m^{-2} d^{-1} over the cruises during Jan. 2015 and Jan. 2017.

i.*Roden et al.* (2013)[18] estimate the annual air-sea CO_2 flux of -6.56 ± 4.33 mmol C m^{-2} d^{-1} in Prydz Bay during May 2010 to Feb. 2011. The mean air-sea CO_2 flux reported by Roden et al. (2016)[93], whose observations were made during austral summer (Jan. to Mar. 2006) at 30−80°E, was -8 ± 21 mmol m^{-2} d^{-1}.

j.*Gibson and Trull* (1999)[51] report the air-sea CO_2 flux of -32.8 mmol m^{-2} d^{-1} during the summer ice-free period (1993−1995).

k.*Shetye et al.* (2017)[86] report Enderby Basin (20°−70°E), which is located in Antarctic coastal region, Indian sector, the average of air-sea CO_2 flux is -28.4 ± 45.6 mmol C m^{-2} d^{-1} from 2009 to 2012 (Mar. 2009, Feb. 2010, Jan. 2012). Along west of 55°E, CO_2 fluxes averaged -6.8 mmol m^{-2} d^{-1} and -5.9 mmol C m^{-2} d^{-1} during February and March, here we take the mean value -6.35 ± 0.64 mmol C m^{-2} d^{-1} as the air-sea CO_2 fluxe of the western Indian Sector.

l.*Murakami et al.* (2020)[19] report the mean air-sea CO_2 flux, -6.5 ± 6.9 mmol m^{-2} d^{-1} in Cape Darnley polynya, East Antarctica (66–68°S,

67–71°E) from 22 to 27 January 2009.

m.*Wang et al.* (2021)[87] report a mean CO_2 flux is −21.40 ± 27.3 mmol m^{-2} d^{-1} during Feb. 2015. The ice-free period is three months per year with 0.08×10^6 km^2.

n.*Tortell et al.* (2012)[88] report an overall mean air-sea CO_2 flux of −15.9 ± 13.8 mmol C m^{-2} d^{-1} (11 Jan to 16 Feb 2009). A mean polynya size is 5.00×10^4 km^2, the open water of AP and PIP during 2008−2009 is exhibited for ~145 days.

o.*Mu et al.* (2014)[89] report an overall mean air-sea CO_2 flux of Amundsen Sea Polynya, −18.0 ± 14.0 mmol C m^{-2} d^{-1}, during austral summer 2010−2011. the average open water area of the ASP from 1997−2010 is 27.3×10^3 km^2.

p.*Álvarez et al.* (2002)[90] report a mean CO_2 flux of the Bellingshausen Sea, −6.5 ± 6 and −4 ± 2.6 mmol m^{-2} d^{-1}, and a mean CO_2 flux of the Gerlache Strait −3.8 ± 4.2 and −15.9 ± 13.7 mmol m^{-2} d^{-1} during austral summer 1995−96.

q.*Legge et al.* (2015)[91] report a net sink of atmospheric CO_2 of −0.56~−1.34 mol C m^{-2} yr^{-1} (average of 3 years, 2011−2013). Here we take the average value of −0.90 ± 0.55 mol C m^{-2} yr^{-1} and assume that the mean daily open water area of the Ryder Bay, west Antarctic Peninsula (WAP) is 1.20×10^2 km^2.

r.*Ito et al.* (2018)[92] report the CO_2 flux of −1.00, 0.20, −2.40 mmol CO_2 m^{-2} d^{-1} in Northern Antarctic Peninsula (including Bransfield, Weddell Sea, Drake Passage) during three summer periods (2008-2010), here we take the average of three years as the mean flux −1.07 ± 1.30 mmol CO_2 m^{-2} d^{-1}, based on the 0.32×10^6 km^2 in the summers of 2008−2010.

s.*Tozawa et al.* (2021)[95] report a mean CO_2 flux is −8.30 ± 12.7 mmol m^{-2} d^{-1} during Dec. 2018 to Jan. 2019.

*The areas of global ocean and global coastal seas are referred to Bauer et al., (2013)[3].

Extended Data Table 2 and C_{ant} export flux around Pan-Antarctic.

Areas	Ventilation rates of DSW (Sv)*	C_{ant} in DSW-TrOCA (μmol kg^{-1})†	C_{ant} in DSW-ΔC* (μmol kg^{-1})$	C_{ant} in mCDW-TrOCA (μmol kg^{-1})†	C_{ant} in in AABW-TrOCA (μmol kg^{-1})†	C_{ant} gross export flux (Tg C yr^{-1})♯	C_{ant} net export flux (Tg C yr^{-1})♯	CO_2 uptake (Tg C yr^{-1}) **	C_{ant} net export/ CO_2 uptake (%)***
Prydz Bay	0.26~0.78	24 ± 14	21 ± 13	20 ± 10	15 ± 3	2.41~7.23	0.40~1.21	−3.86 ± 2.71	10~31
Weddell Sea	1.50~2.50	27 ± 6	22 ± 6	13 ± 9	14 ± 4	15.90~26.50	8.06~13.4	−4.01 ± 1.73	201~335
Ross Sea	0.05~1.91	28 ± 5	11 ± 4	19 ± 6	14 ± 4	0.54~20.70	0.18~6.90	−8.74 ± 2.59	2~79
Adélie Land	0.10~0.50	45 ± 4	30 ± 4	21 ± 8	19 ± 4	1.76~8.81	0.93~4.64	−3.37 ± 1.58	28~138
Cold Shelves‡	1.91~5.69	31 ± 7	21 ± 7	18 ± 8	16 ± 4	20.6~63.2	9.6~26.2	−26.8 ± 8.6	36~98
Pan-Antarctic	3.70~7.10	31 ± 7	21 ± 7	18 ± 8	16 ± 4	44.7~85.8	18.3~35.2	−44.0 ± 11.6	41~78
Coastal Sea								−200‖	

Note: *Ventilation rates of DSW. DSW ventilation rate in southern Weddell Sea is 1.6 ± 0.5 Sv[96] and the rate in western Weddell Sea is 0.4 Sv[97], the total ventilation rate of DSW is 1.5~2.5 Sv; DSW ventilation rates in Ross Sea is 0.98 ± 0.93 Sv according to Whitworth and Orsi (2006)[98]; Williams (2010)[99] has been reported that the DSW ventilation rate in Adélie and George V Land coastal is 0.1~0.5 Sv; Ohshima (2013)[30] has been estimated the DSW ventilation rate of 0.52 ± 0.26 Sv in Prydz Bay (including Cape Darnley regions). The total ventilation rate of DSW is the sum of rates in the four regions above. DSW ventilation rate of 5.4 ±1.7 Sv in Pan-Antarctic shelf regions refers to Orsi (2002)[33];

†The annual means of C_{ant} in DSW, mCDW and AABW are based on the TrOCA method and calculated by the parameters (DIC, TA, O_2, θ) from GLODAPv2.2020 dataset (see "Anthropogenic CO_2 calculation – TrOCA approach" in Methods).

$The annual means of C_{ant} in DSW are based on the ΔC* method and calculated by the parameters (DIC, TA, O_2, θ) from GLODAPv2.2020 dataset (see "Anthropogenic CO_2 calculation –ΔC* approach" in Methods).

‡ For different water masses, C_{ant} in cold shelves is the means of that in Adélie Land, Weddell Sea, Ross Sea, Prydz Bay, which also represents the C_{ant} in Pan-Antarctic.

‖The C_{ant} flux of global coastal sea, −200 Tg C yr^{-1}, is taken from the Roobaert (2019)[1].

♯The range of export fluxes is estimated by C_{ant} values from TrOCA.

**The CO_2 uptake flux of Pan-Antarctic, −1.56 mol C m^{-2} yr^{-1}, is filter out by latitude (>60°S) in Extended Data Table 1 and the area of Pan-Antarctic is adopt from Laruelle (2014)[56], 2.95×10^6 km^2. Negative value means ocean uptake CO_2 from the atmosphere.

***CSP efficiency is the ratio of C_{ant} net export flux to the CO_2 uptake flux.

941
942

Supplementary Files

This is a list of supplementary files associated with this preprint. Click to download.

- CSPAntarcticSOMfinal.pdf